JACS
JOURNAL OF THE AMERICAN CHEMICAL SOCIETY
Article
pubs.acs.org/JACS

Rapid Reduction of the Diferric-Peroxyhemiacetal Intermediate in Aldehyde-Deformylating Oxygenase by a Cyanobacterial Ferredoxin: Evidence for a Free-Radical Mechanism

Lauren J. Rajakovich,[†] Hanne Nørgaard,[‡,§] Douglas M. Warui,[‡] Wei-chen Chang,[‡] Ning Li,[†,⊥] Squire J. Booker,*[,†,‡] Carsten Krebs,*[,†,‡] J. Martin Bollinger, Jr.,*[,†,‡] and Maria-Eirini Pandelia*[,‡]

[†]Department of Biochemistry and Molecular Biology and [‡]Department of Chemistry, The Pennsylvania State University, University Park, Pennsylvania 16802, United States

Supporting Information

ABSTRACT: Aldehyde-deformylating oxygenase (ADO) is a ferritin-like nonheme-diiron enzyme that catalyzes the last step in a pathway through which fatty acids are converted into hydrocarbons in cyanobacteria. ADO catalyzes conversion of a fatty aldehyde to the corresponding alk(a/e)ne and formate, consuming four electrons and one molecule of O_2 per turnover and incorporating one atom from O_2 into the formate coproduct. The source of the reducing equivalents in vivo has not been definitively established, but a cyanobacterial [2Fe-2S] ferredoxin (PetF), reduced by ferredoxin−NADP$^+$ reductase (FNR) using NADPH, has been implicated. We show that both the diferric form of *Nostoc punctiforme* ADO and its (putative) diferric-peroxyhemiacetal intermediate are reduced much more rapidly by *Synechocystis sp.* PCC6803 PetF than by the previously employed chemical reductant, 1-methoxy-5-methylphenazinium methyl sulfate. The yield of formate and alkane per reduced PetF approaches its theoretical upper limit when reduction of the intermediate is carried out in the presence of FNR. Reduction of the intermediate by either system leads to accumulation of a substrate-derived peroxyl radical as a result of off-pathway trapping of the C2-alkyl radical intermediate by excess O_2, which consequently diminishes the yield of the hydrocarbon product. A sulfinyl radical located on residue Cys71 also accumulates with short-chain aldehydes. The detection of these radicals under turnover conditions provides the most direct evidence to date for a free-radical mechanism. Additionally, our results expose an inefficiency of the enzyme in processing its radical intermediate, presenting a target for optimization of bioprocesses exploiting this hydrocarbon-production pathway.

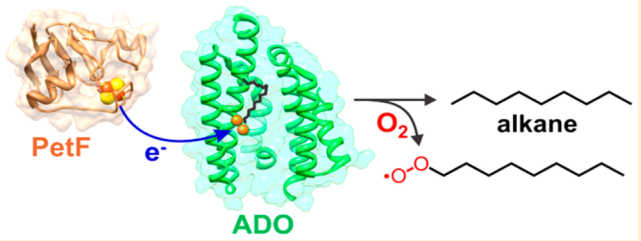

INTRODUCTION

Cyanobacteria harness sunlight for reductive fixation of carbon dioxide, thereby storing light energy in the chemical bonds of biomolecules such as fatty acids. It was recently discovered that, in these microbes, abundant C_n-fatty acids (n = 14, 16, 18) serve as the primary substrates for the production of petrodiesel hydrocarbons, specifically the corresponding C_{n-1} linear alkanes and alkenes.[1] In the first step of this pathway, the enzyme acyl−acyl carrier protein (acyl-ACP) reductase (AAR) cleaves the thioester of its fatty acyl-ACP substrate to produce a fatty aldehyde, thereby providing the substrate for the second enzyme, aldehyde-deformylating oxygenase (ADO).[1−3] ADO converts the carbonyl group of the aldehyde to formate, yielding the C_{n-1} alk(a/e)ne.[1,4,5] An in-depth understanding of these two reactions, their enzyme catalysts, and the cooperation of the enzymes[3] could facilitate ongoing efforts within the biotechnology industry to deploy the pathway for production of diesel fuel in cyanobacteria and heterologous hosts such as *Escherichia coli* (*Ec*).[6−8]

ADO belongs to the ferritin-like diiron-carboxylate oxygenase and oxidase (FDCOO) protein structural superfamily. Members of this superfamily use the reduced (II/II) state of a nonheme-diiron cofactor to activate O_2, most commonly resulting in a two-electron oxidation of the primary substrate via either an early μ-peroxo-$Fe_2^{III/III}$ adduct or a high-valent (e.g., $Fe_2^{IV/IV}$) successor. In the course of substrate oxidation, the cofactor is also oxidized by two electrons in the balanced four-electron reduction of O_2 to the oxidation state of two water molecules. For this reason, FDCOOs generally require an auxiliary reducing system to convert the $Fe_2^{III/III}$ product form of the cofactor generated in each oxidative half-cycle back to the O_2-reactive $Fe_2^{II/II}$ state.

ADO is unique among known FDCOOs in its use of the conserved diiron cofactor for a reaction (cleavage of an aldehyde to formate and an alk(a/e)ne) that at first glance appears to be redox-neutral (hydrolytic).[4,5,9] Our published analysis of the reaction revealed its hidden analogy to other FDCOO reactions by establishing that it shares the usual requirements for both electrons and O_2, with incorporation of one atom of O_2 into the formate product.[4,5,9] However, because ADO does not, by contrast to the other FDCOOs, oxidize its

Received: June 18, 2015
Published: August 18, 2015

DOI: 10.1021/jacs.5b06345
J. Am. Chem. Soc. 2015, 137, 11695−11709

primary substrate, electrons are required from an accessory reducing system not only for cofactor reduction at the end of the substrate conversion half-cycle (the usual two electrons) but also during substrate conversion itself (two *additional* electrons).

In our previous studies, we proposed a free-radical mechanism for the cryptically redox oxygenation reaction catalyzed by ADO (Scheme 1).[5,10] The first step in the mechanism, addition of O_2 in bridging mode to the $Fe_2^{II/II}$ cofactor in the ADO·aldehyde complex to form a μ-peroxo-$Fe_2^{III/III}$ intermediate (**B**), is analogous to early steps demonstrated or proposed in the reactions of other FDCOOs.[11−14] The geometry of the resultant μ-peroxo-$Fe_2^{III/III}$ complex shown in Scheme 1 is just one of several possibilities. The initial O_2 adduct in ADO might well be structurally distinct from the peroxide-level intermediates in other FDCOOs to enable the novel reactivity, attack of the O_2-derived ligand on the aldehyde carbonyl to form a $Fe_2^{III/III}$-peroxyhemiacetal (PHA) intermediate (**C**), required to rationalize the reaction outcome. Reductive cleavage of the O−O bond in **C** would generate a *gem*-diolyl substrate radical (**D**) that could undergo β-scission of the C1−C2 bond, forming a C2-alkyl radical intermediate (R•) and the C1-derived coproduct, formate (**E**). Abstraction of a hydrogen atom (H•) by the alkyl radical from either an amino acid donor in the active site or, as recent data suggest,[15] a coordinated solvent ligand would form the product hydrocarbon along with either an amino acid radical or an $Fe_2^{III/IV}$ form of the cofactor (**F**). Subsequent transfer of a second electron from the reducing system (and probably a proton) and alkane release would result in the formate-bound $Fe_2^{III/III}$ state (**G**). Release of formate, two-electron reduction of the product μ-oxo-$Fe_2^{III/III}$ cofactor back to the $Fe_2^{II/II}$ state, and binding of another aldehyde molecule would prepare the enzyme for the next turnover (**A**).

Scheme 1. Proposed Free-Radical Mechanism[5,10] for ADO Catalysis[a]

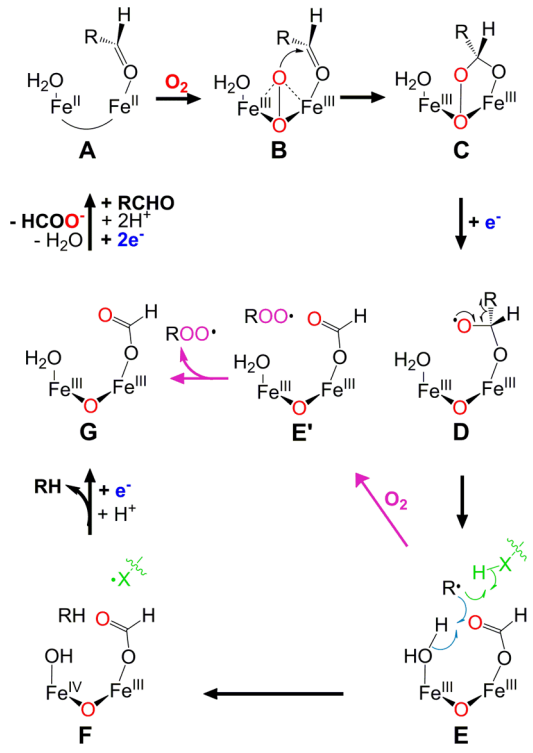

[a]The productive catalytic pathway is shown with black arrows. The unproductive reaction path described in this work is highlighted in magenta.

Two key features of the proposed ADO mechanism are (i) provision by the reducing system of a total of four electrons at three distinct stages of the catalytic cycle and (ii) C1−C2 bond cleavage by a free-radical mechanism to generate R• as a precursor to the hydrocarbon product. Indirect evidence for formation of the proposed R• was provided in two separate studies employing radical-trapping substrate analogues.[16,17] However, another study implied that pathways involving heterolytic bond cleavage steps might also be possible.[18] For provision of the required electrons, the published in vitro studies of the ADO reaction have employed a ferredoxin/ferredoxin−$NADP^+$ reductase system with NADPH (Fd/FNR/N) or a small molecule mediator, specifically phenazine methosulfate or 1-methoxy-5-methylphenazinium methyl sulfate (^{MeO}PMS), chemically reduced by NADH or sodium dithionite.[9,10,19] The phenazine system was shown to afford only half the theoretical yield of products with respect to reducing equivalents.[10] This inefficiency was attributed to uncoupled or improperly timed electron delivery to the diiron site by the two-electron reductant. The heterologous spinach Fd/FNR/N system was found to support very few ADO turnovers in vitro.[4,20] However, improved activity was demonstrated for *Synechococcus elongatus* PCC7942 (*Se*) ADO with its cognate Fd/FNR/N system and in the context of a *Se* ADO-Fd-FNR fusion protein.[20,21] The latter studies suggested the possibility that this system might be a physiologically relevant ADO reductant, but no in-depth analysis of electron delivery was reported. Consequently, details of how ADO and its reducing partner ensure the orderly transfer of a total of *four* electrons at multiple points in the catalytic cycle have not yet been elucidated, a significant gap in our understanding of the ADO mechanism.

In this work, we have sought to fill the existing gaps in both the evidence for a free-radical mechanism and our understanding of electron delivery in the ADO reaction. By analogy to published experiments employing the chemical reducing system,[10] we examined the efficacy of electron delivery by a [2Fe-2S] Fd, PetF, from the model cyanobacterium *Synechocystis sp.* PCC6803 (*Syn.* 6803) together with its cognate FNR (encoded by the *ssl0020* and *slr1643* genes, respectively) in catalysis by *Nostoc punctiforme* (*Np*) ADO. The reductions of the $Fe_2^{III/III}$ state and the (putative) $Fe_2^{III/III}$−PHA intermediate by this system are both much faster than those by the phenazine reductant. Reduction of the $Fe_2^{III/III}$−PHA intermediate by the PetF/FNR/N system is also more tightly coupled to C1−C2 fragmentation, resulting in yields of formate and (under proper conditions) alkane that approach their theoretical upper limits with respect to reducing equivalents. We also show that the rapid reduction of the $Fe_2^{III/III}$−PHA intermediate by the single-electron donor, PetF, allows for accumulation of a substrate-derived radical species, which also accumulates, but to a lesser extent, following the more sluggish reduction of the intermediate by ^{MeO}PMS. The spectroscopic properties of this radical and its greater accumulation in the presence of excess O_2 suggest that it is a peroxyl radical. Its accumulation correlates with the diminished yield of the reduced hydrocarbon product, indicating that it is formed by the addition of O_2 to the R• in competition with productive quenching by H• transfer. The rapid formation of this radical

DOI: 10.1021/jacs.5b06345
J. Am. Chem. Soc. 2015, 137, 11695−11709

upon reduction of the $Fe_2^{III/III}$–PHA intermediate and in competition with formation of the hydrocarbon product provides the strongest evidence yet reported for a free-radical mechanism. These results expose the limited capacity of the enzyme to manage its R• intermediate, particularly in the case of short-chain substrates, and provide an explanation for previous reports of diminished hydrocarbon productivity at high concentrations of O_2.[17,22] This vulnerability may represent a target for directed improvement in efforts to deploy the enzyme in fuel-producing bioprocesses.

EXPERIMENTAL SECTION

Materials. Technical grade (>85% purity) sodium hydrosulfite (dithionite), β-nicotinamide adenine dinucleotide phosphate, reduced disodium salt hydrate (≥97%) (NADPH), 2-nitrophenylhydrazine (97%) (2-NPH), sodium chlorite ($NaClO_2$), spinach ferredoxin, spinach ferredoxin–$NADP^+$ reductase, *n*-hexadecane, and short-chain aldehyde substrates (*n*-octanal and *n*-decanal) were purchased from Sigma-Aldrich (St. Louis, MO). 1-(3-(Dimethylamino)propyl)-3-ethylcarbodiimide (98%) (EDC) was purchased from Alfa Aesar (Ward Hill, MA). 1-Methoxy-5-methylphenazinium methyl sulfate (^{MeO}PMS) was obtained from Acros Organics (Morris Plains, NJ). *n*-Octadecanal and *n*-1-[^{13}C]-octanal were synthesized according to previously described procedures.[1,4] *n*-1-[^{13}C]-Stearoyl-ACP was prepared according to a previously published procedure.[3] Procedures for syntheses of 2,2-[^{2}H]$_2$-decanal, 1-[^{2}H]-decanal, 3-thiadecanal, and 2,2-[^{2}H]$_2$-3-thiadecanal are provided in the Supporting Information (Scheme S1). *n*-1-[^{13}C]-Octadecanoic acid and *n*-1-[^{13}C]-octanoic acid were obtained from Cambridge Isotope Laboratories, Inc. (Andover, MA). All other chemicals used for protein overexpression and purification were purchased from Sigma-Aldrich, unless stated otherwise.

Preparation of *Np* AAR, *Np* ADO, *Syn.* 6803 Fds, *Syn.* 6803 FNR, and *Dechloromonas aromatica* Cld. Detailed protocols for protein overexpression and purification are provided in the Supporting Information.

The concentration of ADO was determined from absorbance at 280 nm by using a molar absorption coefficient of 22 920 $M^{-1}\cdot cm^{-1}$.[10] Iron content was determined by inductively coupled plasma atomic emission spectroscopy (ICP-AES) by Mr. Henry Gong at the Pennsylvania State Materials Research Institute. The concentrations of ADO given are of diiron cluster, calculated as half the measured iron concentration.

PetF protein concentration was determined using a Direct Detect spectrometer (EMD Millipore, Darmstadt, Germany). The fraction of protein containing the reduced $[2Fe\text{-}2S]^{1+}$ cofactor was determined by EPR spin quantification on a protein sample reduced by treatment with 10 mM sodium dithionite (Figure S1). A frozen solution of Cu^{2+}–EDTA was used as the spin concentration standard.[23] The concentrations of PetF given are of the $[2Fe\text{-}2S]^{1+}$ cofactor. Chemically reduced PetF was prepared by O_2-free incubation of the oxidized protein with 10 mM sodium dithionite (>2-fold excess with respect to [PetF] cofactor) at 4 °C for 30 min. The sodium dithionite was removed and the buffer was exchanged by using a PD-10 desalting column (G-25 Sephadex medium, GE Healthcare) equilibrated with O_2-free 50 mM sodium 2-[4-(2-hydroxyethyl)-piperazin-1-yl] ethanesulfonate (HEPES) buffer, pH 7.5.

FNR protein concentration was determined from absorbance at 280 nm by using a molar absorption coefficient of 50 210 $M^{-1}\cdot cm^{-1}$. FNR was reconstituted with equimolar flavin adenine dinucleotide (FAD^+) and filtered through a 30K MWCO Amicon Ultra centrifugal filter (EMD Millipore, Merck KGaA, Darmstadt, Germany) to remove excess FAD^+. The concentration of bound FAD^+ was determined from absorbance at 460 nm by using a molar absorption coefficient of 10 800 $M^{-1}\cdot cm^{-1}$. The concentrations of FNR given are of the FAD^+-bound form.

Stopped-Flow Absorption Spectroscopy (SF-Abs) and Data Analysis. SF-Abs experiments were carried out at 5 °C in an Applied Photophysics Ltd. (Leatherhead, UK) SX20 stopped-flow spectrophotometer, which was housed in an anoxic chamber (Labmaster, MBraun, Stratham, NH). The instrument was configured for sequential-mixing, an optical path length of 1 cm, and data acquisition with white light and the photodiode-array (PDA) detector, unless otherwise indicated. In the first mix, an O_2-free solution containing $Fe_2^{II/II}$–ADO (0.033, 0.050, 0.10, 0.20, 0.40 mM) and 10 mM of either octanal or decanal substrate was mixed with an equal volume of O_2-saturated (1.8 mM at 5 °C) 50 mM sodium HEPES buffer (pH 7.5). This solution was allowed to react for 10, 15, or 20 s to accumulate the $Fe_2^{III/III}$–PHA intermediate, according to the formation kinetics defined in single-mixing experiments employing monochromatic light and a photomultiplier tube (PMT) detector (Figure S2A). This reaction solution was then mixed with an equal volume of a solution containing 0.10 mM chemically reduced PetF. Time-dependent absorption spectra (1000 points) were acquired on a logarithmic time base after the second mixing event. The dead-time of the stopped-flow apparatus is slightly more than 1 ms. Control experiments, in which the $Fe_2^{II/II}$–ADO·aldehyde complex was replaced in the first mixing event with O_2-free buffer, were carried out to define the kinetics of oxidation of PetF by O_2. Additional single-mix experiments were carried out to assess the rate of reduction of the as isolated $Fe_2^{III/III}$–ADO by PetF. Details of reaction conditions are provided in the figure legends.

ΔA_{423}-versus-time traces monitoring PetF $[2Fe\text{-}2S]^{1+}$ oxidation from experiments with varying PetF:ADO ratios (0.5, 1, 2, 4, 6) were fit by sums of exponential functions, eqs 1 and 2, corresponding to parallel first-order reactions with different amplitudes (ΔA_1, ΔA_2, ΔA_3) and observed rate constants (k_1, k_2, k_3), where A_0 is the initial absorbance.

$$\Delta A_{423}(t) = A_0 + \Delta A_1(1 - e^{-k_1 t}) + \Delta A_2(1 - e^{-k_2 t}) \quad (1)$$

$$\Delta A_{423}(t) = A_0 + \Delta A_1(1 - e^{-k_1 t}) + \Delta A_2(1 - e^{-k_2 t}) + \Delta A_3(1 - e^{-k_3 t}) \quad (2)$$

Single-Turnover Assays for Product Detection. Single-turnover ADO assays were performed in the MBraun anoxic chamber. In glass vials, 30 μL of a solution containing 0.25 mM $Fe_2^{II/II}$–ADO and 12.5 mM 1-[^{2}H]-decanal in 5 mM sodium HEPES (pH 7.5) was mixed with 45 μL O_2-saturated (1.8 mM O_2 at 5 °C) or air-saturated (0.28 mM O_2 at 25 °C) 50 mM sodium HEPES (pH 7.5) buffer by rapid injection via a gastight syringe. After being allowed to react for 10 s (O_2-saturated) or 20 s (air-saturated) to accumulate the $Fe_2^{III/III}$–PHA intermediate (Figure S2B), this solution was mixed with an equal volume of reductant solution. In experiments employing PetF as the reductant, the reductant solution contained chemically reduced PetF (as described above). For reactions employing the PetF/FNR/N system, the initial $Fe_2^{II/II}$–ADO·aldehyde solution contained O_2-free, oxidized 0.25 mM PetF and 0.25 mM FNR, and the reductant solution contained NADPH. After mixing with the reductant, the 0.15 mL reactions were rapidly terminated (after ∼1 s) by addition of 0.15 mL of a solution of 40 μM hexadecane internal standard in ethyl acetate, with vigorous vortexing for 30 s. Samples were centrifuged at 16 000*g* for 30 min. The top organic layer containing the alkane product was removed and analyzed on a Shimadzu GCMS-QP5000 gas chromatography mass spectrometer (GC-MS), as previously reported.[4] Alternatively, the reactions were quenched in 30 μL of a solution of 2-NPH and EDC for quantification of the formate coproduct as its 2-NPH derivative, as previously described.[4,5,10] A 1 mM derivatized propionic acid solution (10 μL) was added to each sample as an internal standard. The samples (4 μL injections) were analyzed on a 6410 LC/MS Agilent QQQ spectrometer using a Hamilton PRP-1 analytical column, as previously described.[5,10]

Activity Assays. Reactions of the AAR and ADO coupled system were performed at 37 °C for 1 h. Assays (0.1 mL) contained 10 μM AAR, 20 μM ADO, 0.20 mM 1-[^{13}C]-stearoyl-ACP, 4 mM NADPH, 7.8 μM (spinach or *Syn.* 6803) Fd, and 7.8 μM (spinach or *Syn.* 6803) FNR. Multiple turnover assays with the ADO variants (0.20 mL) were performed at 5 °C for 5 min. Reactions contained 10 μM ADO, 2.5 mM decanal, 0.2 mM ^{MeO}PMS, and 10 mM NADH. Reactions were

DOI: 10.1021/jacs.5b06345
J. Am. Chem. Soc. 2015, 137, 11695–11709

terminated by mixing with an equal volume of a solution of 40 μM hexadecane internal standard in ethyl acetate with vortexing and were then centrifuged at 16 000g for 30 min. The top organic layer containing the aldehyde substrate and alkane product was removed and analyzed on a Shimadzu GCMS-QP5000, as previously reported.[24]

Preparation of Freeze-Quenched Samples for Electron Paramagnetic Resonance (EPR) and Mössbauer Spectroscopies. General procedures for freeze-quench (FQ) EPR and Mössbauer experiments have been published previously.[25−27] Sequential-mixing FQ-Mössbauer experiments were conducted at 5 °C by using three syringes that contained (1) 1.4 mM $^{57}Fe^{II/II}$−ADO, 16.6 mM decanal and 10 μM Cld; (2) 10 mM $NaClO_2$; (3) 1.4 mM chemically reduced PetF. The buffer for all three solutions was 50 mM sodium HEPES, pH 7.5, 10% glycerol. The contents of syringes 1 and 2 were mixed in equal volume, and this solution was allowed to react for 30 s to generate the $Fe_2^{III/III}$−PHA intermediate (Figure S2C). The resultant solution was then mixed with an equal volume of the syringe 3 solution, and this solution was allowed to react for 10 ms before being rapidly frozen (freeze-quenched) in isopentane at −150 °C.

Sequential-mixing FQ-EPR experiments were conducted at 5 °C by using three syringes. In experiments with high O_2 concentrations, the syringes that contained (1) 0.9 mM $Fe_2^{II/II}$−ADO, 16.6 mM octanal or decanal, and 10 μM Cld; (2) 10 mM $NaClO_2$; (3) chemically reduced PetF or 0.45 mM ^{MeO}PMS reduced with 0.23 mM sodium dithionite (again, all in 50 mM sodium HEPES, pH 7.5, 10% glycerol). In experiments with low O_2 concentrations, Cld was omitted from syringe 1, and syringe 2 contained O_2-saturated (1.8 mM O_2) 50 mM sodium HEPES, pH 7.5 buffer, instead of $NaClO_2$. In both cases, solutions 1 and 2 were mixed in equal volume, and the resultant solution was incubated for 30 s to generate the $Fe_2^{III/III}$−PHA intermediate (Figure S2D). This solution was then mixed with an equal volume of the syringe 3 solution, and the resultant solution was incubated for varying times before being freeze-quenched in isopentane at −150 °C. Minor deviations from these general experimental procedures are noted in the appropriate text and figure legends.

Mössbauer Spectroscopy. Mössbauer spectra were recorded on spectrometers described previously[25] from WEB Research (Edina, MN). The spectrometer used to acquire the weak-field spectra was equipped with a Janis SVT-400 variable-temperature cryostat. The external magnetic field was applied parallel to the γ beam. All isomer shifts quoted are relative to the centroid of the spectrum of α-iron metal at room temperature. Simulations of Mössbauer spectra were carried out with the WMOSS spectral analysis software (www.wmoss.org, WEB Research, Edina, MN).

Continuous-Wave (CW) EPR Spectroscopy. X-Band (~9.5 GHz) EPR spectra were acquired on a Bruker ESP-300 spectrometer equipped with an ER/4102 ST resonator (Bruker), an Oxford Instruments continuous helium flow cryostat, and an Oxford Instruments temperature controller (ITC 502). For all experiments, quartz tubes with 3 mm inner and 4 mm outer diameter were used (QSI). The first-derivative EPR spectra were simulated with the MATLAB-based (Mathworks) *EasySpin* simulation software (http://easyspin.org/).[28]

Pulse EPR Spectroscopy. Pulse X-Band (~9.5 GHz) and Q-band (~34 GHz) field-swept EPR spectra and hyperfine sublevel correlation (HYSCORE) spectra were acquired on a Bruker ELEXSYS E580 spectrometer equipped with a home-built intermediate frequency (IF) extension (designed and fabricated by Dr. Alexey Silakov of Penn State University) of the SuperX-FT X-band bridge.[29] Field-swept electron-spin−echo-detected EPR spectra were recorded using the two-pulse echo sequence ($\pi/2-\tau-\pi-\tau-$echo). HYSCORE experiments were recorded with the standard pulse sequence ($\pi/2-\tau-\pi/2-t_1-\pi-t_2-\pi/2$) and were measured at the field positions corresponding to the principal orientations of the **g**-tensor. Simulations of the HYSCORE spectra were carried out with the freely available MATLAB-based software *KAZAN viewer* (https://sites.google.com/site/silakovalexey/kazan-viewer/) developed by Dr. Alexey Silakov (Penn State University) and Prof. Boris Epel (University of Chicago).

Density Functional Theory (DFT) Calculations. Geometry optimizations and single-point energy calculations were carried out with the ORCA software package.[30] The structures of the peroxyl radicals considered were first geometry optimized without any restrictions. The optimized geometries were further used as inputs for the calculations of the EPR parameters (**g**-tensors and **A**-tensors). All calculations were performed with the unrestricted Hartree−Fock method employing the B3LYP density functional. The TZVP basis set was used for all atoms. The conductor-like screening model (COSMO) was employed to account for electrostatic screening by the protein. A dielectric constant (ε) of 4 was assumed, consistent with previous studies.[31] Calculations were performed on both the $C_9H_{18}OO\bullet$ radical and its 2-thia analogue. Calculations were also performed on the R• precursor for purposes of comparison and to provide additional evidence for the favored assignment of the detected species as a peroxyl radical.

RESULTS

Identification of *Syn.* 6803 *ssl0020* Fd, PetF, as an Efficient ADO Reductant. The genome of the cyanobacterium *Syn.* 6803 contains seven genes encoding putative Fds ([2Fe-2S]- or [4Fe-4S]-containing) and one encoding a FNR (FAD-containing).[32] All seven *Syn.* 6803 Fds were heterologously expressed, purified, and assessed in vitro with the recombinantly produced *Syn.* 6803 FNR for the capacity to support turnover by *Np* ADO. Coupled AAR/ADO reactions were carried out to monitor conversion of the stearoyl-ACP substrate to the octadecanal intermediate and finally to the heptadecane product. After a standard incubation of 1 h, the highest heptadecane yield was observed in the presence of the [2Fe-2S] cluster-containing Fd protein encoded by the *Syn.* 6803 *ssl0020* gene, also known as PetF (Figure S3, purple). When PetF was employed, octadecanal was not detected, indicating that all of the aldehyde intermediate produced by AAR was subsequently converted by ADO to heptadecane. Reactions performed with the spinach Fd/FNR system led to lesser heptadecane yields (Figure S3, blue) and accumulation of the aldehyde intermediate, in agreement with previous reports by us[4] and others[20] that this system supports only modest ADO activity. Thus, the cyanobacterial *Syn.* 6803 *ssl0020* Fd, PetF, was selected for use in single-turnover experiments on the basis of its ability to support the greatest ADO activity.

Verification That Reduction of the $Fe_2^{III/III}$−PHA Intermediate by PetF/FNR/N Is Productive. Two electrons are required for productive reduction of the $Fe_2^{III/III}$−PHA intermediate to formate and alkane. Thus, with a sample containing only the intermediate form of the enzyme, the theoretical reaction stoichiometry would be 2:1 PetF:ADO. To determine the experimental stoichiometry, the C1-derived product, formate, was quantified in manually chemically quenched samples prepared by treatment of the preformed intermediate with varying molar ratios of a reductant. With the chemically reduced PetF as reductant, a stoichiometry of 0.58 equiv of formate per 2 equiv of PetF (two electrons) was obtained (Figure 1, blue). This value deviates from the theoretical stoichiometry (1 formate per 2 electrons), demonstrating an uncoupling of electron delivery and product formation, as previously observed with the phenazine reductant.[10] In contrast, when FNR was included in equimolar quantity with PetF and ADO and the two-electron donor NADPH was used as the electron source, the experimental stoichiometry increased to 0.96 formate per 2 electrons (Figure 1, black), very close to the theoretical value. Thus, the

DOI: 10.1021/jacs.5b06345
J. Am. Chem. Soc. 2015, 137, 11695−11709

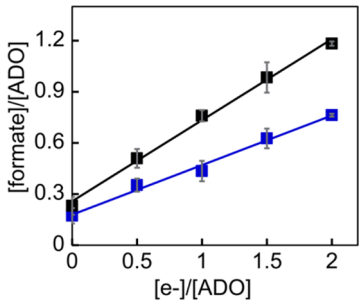

Figure 1. Formate production in single-turnover ADO assays utilizing different reducing systems. The accumulated $Fe_2^{III/III}$–PHA intermediate was reacted for ~1 s with varying molar ratios of reductant: either chemically reduced PetF (blue) or NADPH (black) in the presence of oxidized PetF and oxidized FNR in equimolar ratios with ADO (0.050 mM final). Data are averages of at least three replicate assays.

reduction of the $Fe_2^{III/III}$–PHA intermediate via the PetF/FNR/N system is tightly coupled to product formation.

SF-Abs Evidence for Rapid Reduction of the $Fe_2^{III/III}$–PHA Intermediate by PetF. The kinetics of the reaction of the $Fe_2^{III/III}$–PHA intermediate with reduced PetF were monitored by sequential-mixing SF-Abs spectroscopy (Figure 2). In the first mix, the $Fe_2^{II/II}$–ADO·aldehyde complex was reacted with O_2-saturated buffer to permit maximal accumulation of the $Fe_2^{III/III}$–PHA intermediate (Figure S2A),[10] which was then reacted in a second mix with chemically reduced PetF. Time-dependent absorption spectra obtained after the second mix (Figure 2A) reflect, primarily, oxidation of the $[2Fe\text{-}2S]^{1+}$ form of PetF to the $[2Fe\text{-}2S]^{2+}$ form (increasing absorption at 330, 423, and 465 nm; see also Figure S4A).

The ADO concentration was varied at a constant PetF concentration in order to delineate the kinetics of oxidation of the $[2Fe\text{-}2S]^{1+}$ cluster in PetF by the $Fe_2^{III/III}$–PHA intermediate and the $Fe_2^{III/III}$ cluster forms. For all ratios of PetF:ADO examined, the same overall change in absorbance at 423 nm was observed (Figure 2B). This constant value of ΔA_{423} (0.18) is consistent with complete PetF oxidation (Figure S4B). However, as expected, the kinetics of oxidation depend on whether the ADO intermediate is present at sufficiently high concentration to oxidize the PetF entirely itself (at low PetF:ADO) or, alternatively, the product $Fe_2^{III/III}$ cluster and/or additional turnovers must also contribute to PetF oxidation (at high PetF:ADO).

Experiments with PetF:ADO ≤ 2. In the experiments with either 0.5:1 or 1:1 PetF:ADO (Figure 2B, blue and pink traces), the kinetic traces had a high initial absorbance, demonstrating that the majority of the PetF undergoes oxidation within ~1 ms (the dead-time of the measurements). This oxidation is illustrated by comparison of the PetF absorption spectrum at 1 ms to the mathematically generated spectrum for time zero (Figure 2A, purple and black traces). Due to this limitation in data acquisition, the kinetics of PetF oxidation in these reactions could not be reliably analyzed. Nevertheless, a lower limit of >500 s^{-1} could be set for the apparent first-order rate constant of this rapid oxidation. A slow exponential decay phase was also observed, most discernible in the trace from the experiment with 0.5 equiv of PetF:ADO (Figure 2B, blue trace). The observed decay rate constant, k_{obs} = 0.017 s^{-1}, correlates well with that reported for the unproductive decay of the $Fe_2^{III/III}$–PHA intermediate (λ_{max} = 450 nm) to a μ-oxo-$Fe_2^{III/III}$ species (λ_{max} = 350 nm) under the intense, polychromatic incident light employed in this experiment.[10]

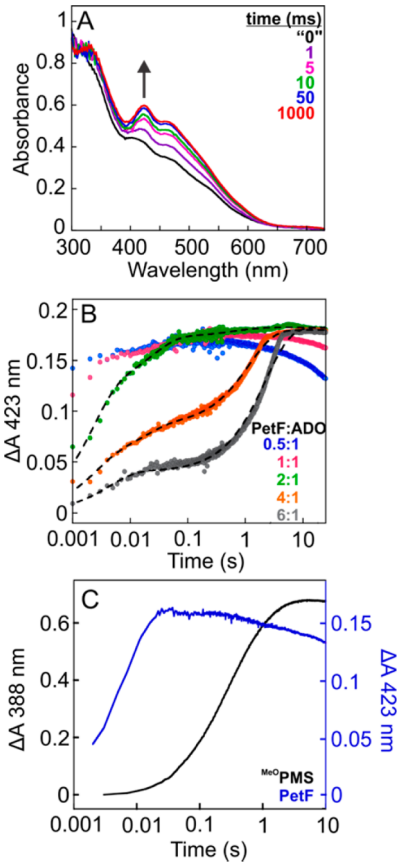

Figure 2. Sequential-mixing SF-Abs experiments monitoring PetF oxidation upon reaction with the $Fe_2^{III/III}$–PHA intermediate. (A) Time-dependent absorption spectra after mixing the accumulated $Fe_2^{III/III}$–PHA intermediate with 2 equiv of chemically reduced PetF (0.050 mM final). The $Fe_2^{III/III}$–PHA intermediate was generated by mixing the $Fe_2^{II/II}$–ADO·octanal complex with O_2-saturated buffer and incubating for 15 s. The "0" ms reference spectrum was constructed mathematically by addition of the spectra of the chemically reduced PetF and the $Fe_2^{III/III}$–PHA intermediate (Figure S4C). (B) Kinetic traces monitoring PetF $[2Fe\text{-}2S]^{1+}$ oxidation by the increase in absorption at 423 nm in experiments in which the ADO concentration was varied at a constant concentration of chemically reduced PetF (0.050 mM final). Dashed lines are the fits described in the Experimental Section. (C) Comparison of the kinetics of oxidation of 2 equiv of PetF (λ = 423 nm) or 1 equiv of ^{MeO}PMS (λ = 388 nm)[10] upon reaction with the $Fe_2^{III/III}$–PHA intermediate. The intermediate was accumulated by mixing a solution of 0.1 or 0.3 mM $Fe_2^{II/II}$–ADO (PetF or ^{MeO}PMS experiment, respectively) and 10 mM decanal with an equal volume of O_2-saturated buffer and incubating for 15 s before the second mixing event.

In the experiment with 2:1 PetF:ADO (Figure 2B, green trace), the kinetic trace was best fit by a sum of two exponential functions with observed rate constants of 460 s^{-1} and 42 s^{-1} and amplitudes of ΔA_{423} = 0.12 and 0.051, respectively. These rate constants are significantly greater than those associated with the slow oxidation of PetF observed in control experiments in which ADO was either used in its as-isolated μ-oxo-$Fe_2^{III/III}$ form (Figure S5A) or omitted entirely (Figure S4B). These results establish that the rapid oxidation of PetF with PetF:ADO ≤ 2 is mediated by the $Fe_2^{III/III}$–PHA intermediate.

DOI: 10.1021/jacs.5b06345
J. Am. Chem. Soc. 2015, 137, 11695–11709

Experiments with PetF:ADO > 2. With 4 equiv of PetF:ADO (Figure 2B, orange trace), the kinetic trace could be fit by an equation for three parallel exponential processes. Rapid oxidation of approximately half of the PetF (ΔA_{423} = 0.085) occurred with observed rate constants of 440 s^{-1} and 56 s^{-1}. These rate constants are comparable to those observed with 2:1 PetF:ADO, indicating that this fast phase represents oxidation of 2 equiv of PetF by the $Fe_2^{III/III}$–PHA intermediate. The remaining half of the PetF (ΔA_{423} = 0.094) was oxidized with a markedly diminished observed rate constant, 0.86 s^{-1}. Control SF-Abs experiments, in which as-isolated μ-oxo-$Fe_2^{III/III}$–ADO was reacted with reduced PetF (Figure S5), gave a comparable rate constant of 0.81 s^{-1}, demonstrating that this slow phase represents reduction of the $Fe_2^{III/III}$ cofactor to the $Fe_2^{II/II}$ state. When the PetF:ADO ratio was further increased to 6:1 (Figure 2B, gray), similar fast and slow kinetic phases were observed [k_{obs1} = 230 s^{-1} and k_{obs2} = 0.44 s^{-1}]. The complete oxidation of PetF observed in this experiment with excess O_2 and aldehyde substrate is explained by the completion of one full catalytic cycle, which consumes 4 equiv of PetF, followed by a second half-turnover, in which the remaining PetF is oxidized.

Reduction of the $Fe_2^{III/III}$–PHA Intermediate by PetF Monitored by FQ-Mössbauer. FQ-Mössbauer experiments were performed to monitor reduction of the $Fe_2^{III/III}$–PHA intermediate by PetF and identify any intermediates that may accumulate during this reaction. In an initial single-mixing experiment, the $^{57}Fe_2^{II/II}$–ADO·decanal complex was reacted for 30 s with the O_2-generating chlorite dismutase/chlorite (Cld/$NaClO_2$) enzymatic system to accumulate the $Fe_2^{III/III}$–PHA intermediate to a maximum extent (see Figure S2C for the corresponding SF-Abs experiment).[10,33,34] The Mössbauer spectrum of this sample (Figure 3A, black bars) is dominated by the pair of partially resolved quadrupole doublets associated with the site-differentiated $Fe_2^{III/III}$–PHA intermediate. The parameters for the individual sites are δ_1 = 0.48 mm/s, ΔE_{Q1} = 0.49 mm/s (gray bracket) and δ_2 = 0.55 mm/s, ΔE_{Q2} = 1.23 mm/s (black bracket).[10] The spectrum of the intermediate accounts for 80% of the total iron absorption area, as determined by using the previously published[10] experimental reference spectrum (red line). The remaining absorption area arises from a quadrupole doublet with parameters $\delta \sim 1.3$ mm/s, $\Delta E_Q \sim 3.0$ mm/s (blue line), attributable to the ~20% of substrate-free $Fe_2^{II/II}$–ADO in the sample.[10]

In a subsequent experiment, the $Fe_2^{III/III}$–PHA intermediate generated in the same manner was then reacted for 0.010 s with 2 equiv of chemically reduced unlabeled (>95% ^{56}Fe) PetF. The spectrum of this sample (Figure 3B) does not exhibit the well-resolved features associated with the $Fe_2^{III/III}$–PHA intermediate, suggesting that the intermediate has mostly reacted with the reduced PetF. The accumulation of a new species upon reaction of the $Fe_2^{III/III}$–PHA intermediate with reduced PetF for 0.010 s was demonstrated in the following way. Spectrum A was subtracted from spectrum B to yield a difference spectrum (Figure 3C, black bars), in which the lines pointing upward represent the features of the $Fe_2^{III/III}$–PHA intermediate that decay. Adding back 55% of the experimental reference spectrum of the $Fe_2^{III/III}$–PHA intermediate (Figure 3C, red line) to this difference spectrum cancels the features of the decayed $Fe_2^{III/III}$–PHA intermediate and yields the spectrum of the new species that form (Figure 3D). The significant overlap of the various subspectra makes the fraction of intensity from the $Fe_2^{III/III}$–PHA intermediate to add back

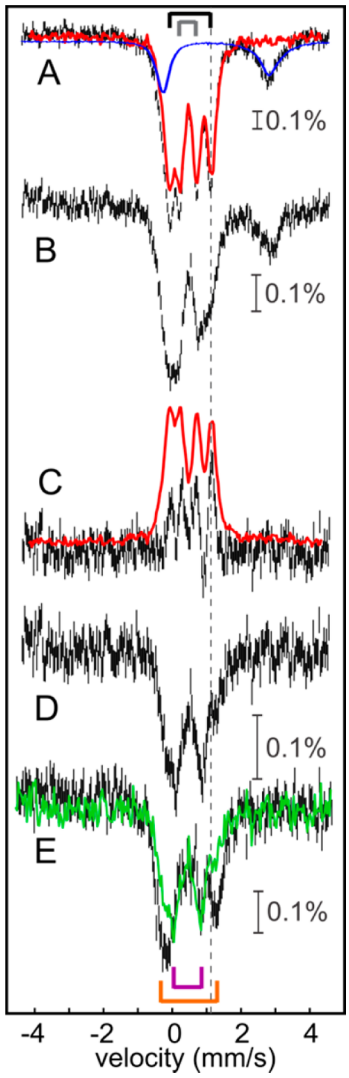

Figure 3. 4.2-K/53-mT FQ-Mössbauer spectra monitoring the reaction of the $Fe_2^{III/III}$–PHA intermediate with 2 equiv of reduced PetF. (A) Spectrum of the $Fe_2^{III/III}$–PHA intermediate accumulated after a solution of the $^{57}Fe_2^{II/II}$–ADO·decanal complex and Cld was reacted with $NaClO_2$ for 30 s. The previously published experimental reference spectrum of the $Fe_2^{III/III}$–PHA intermediate[10] is overlaid in red with the constituent quadrupole doublets designated with black and gray brackets. The experimental reference spectrum of substrate-free $Fe_2^{II/II}$–ADO is overlaid in blue. (B) Spectrum of a sample quenched after reaction of the $Fe_2^{III/III}$–PHA intermediate with 2 equiv of chemically reduced unlabeled (>95% ^{56}Fe) PetF for 0.010 s. The dashed line denotes the high-energy line of the doublet with ΔE_Q = 1.2 mm/s (black bracket) arising from the $Fe_2^{III/III}$–PHA intermediate. (C) B–A difference spectrum (black bars), overlaid with 55% of the experimental reference spectrum of the $Fe_2^{III/III}$–PHA intermediate (red line).[10] (D) Experimental reference spectrum of the $Fe_2^{III/III}$ clusters formed upon reaction of the $Fe_2^{III/III}$–PHA intermediate with 2 equiv of reduced PetF for 0.010 s. The spectrum was generated by addition of 55% of the experimental reference spectrum of the $Fe_2^{III/III}$–PHA intermediate to the difference spectrum C. (E) Experimental reference spectrum of the $Fe_2^{III/III}$ clusters generated upon reaction of the $Fe_2^{III/III}$–PHA intermediate with 2 equiv of reduced PetF for 0.22 s (black bars; see Figure S7 for generation of the spectrum). The derived spectrum of the $Fe_2^{III/III}$ species formed after the 0.010 s reaction with PetF is overlaid for comparison (green line) to depict the changes in relative intensity of the doublets of the two $Fe_2^{III/III}$ forms ($\delta \approx 0.5$ mm/s with $\Delta E_Q \approx 0.8$ and 1.5 mm/s, purple and orange brackets, respectively).

DOI: 10.1021/jacs.5b06345
J. Am. Chem. Soc. 2015, 137, 11695–11709

rather uncertain (55 ± ~ 8%); however, varying its contribution within this limited range does not drastically change the resultant reference spectrum of the new species (Figure S6). The spectrum shown in Figure 3D can be rationalized as the superposition of two (or more) broad and overlapping quadrupole doublets with parameters typical of antiferromagnetically (AF)-coupled $Fe_2^{III/III}$ clusters (Figure S6).

The Mössbauer spectrum of a sample obtained after reaction of the $Fe_2^{III/III}$–PHA intermediate with reduced PetF for a longer time (t = 0.22 s) was analyzed in an analogous fashion (Figure S7), and the derived reference spectrum of the $Fe_2^{III/III}$ clusters that form is shown in Figure 3E (black bars). This spectrum was generated under the assumption of complete reduction of the $Fe_2^{III/III}$–PHA intermediate. Direct comparison to the reference spectrum of the $Fe_2^{III/III}$ clusters obtained after 0.010 s reaction time (Figure 3E, green line) reveals that the relative amounts of the (at least) two different $Fe_2^{III/III}$ clusters change between 0.010 and 0.22 s. The relative quantity of $Fe_2^{III/III}$ cluster(s) characterized by smaller quadrupole splitting ($\Delta E_Q \approx 0.8$ mm/s, purple bracket) decreases, whereas the quantity of the $Fe_2^{III/III}$ cluster(s) with larger quadrupole splitting ($\Delta E_Q \approx 1.5$ mm/s, orange bracket) increases. Though the spectral resolution is insufficient to confidently assign these $Fe_2^{III/III}$ forms to specific intermediates in the ADO reaction, their spectroscopic features are similar to those reported for the purported formate-bound $Fe_2^{III/III}$ cluster (state **G** in Scheme 1),[10] consistent with the productive reduction of the $Fe_2^{III/III}$–PHA intermediate by PetF in less than 0.22 s.

Evidence for Rapid Transfer of a Second Electron to ADO Following Reduction of the $Fe_2^{III/III}$–PHA Intermediate. The results of SF-Abs experiments with PetF:ADO ≤ 1 imply that an appreciable fraction of $Fe_2^{III/III}$–PHA intermediate was not reduced under these conditions (Figure 2B), raising the possibility that the reaction kinetics of reductive C1–C2 bond cleavage might favor rapid transfer of a second electron to the same ADO molecule after the initial reduction of the $Fe_2^{III/III}$–PHA intermediate. This hypothesis was tested in a FQ-Mössbauer experiment in which a sample containing ~65% of the $Fe_2^{III/III}$–PHA intermediate (Figure 4A) was mixed with 0.5 equiv of reduced PetF and allowed to react for 0.22 s (Figure 4B, black bars). This reaction time was chosen to ensure complete PetF oxidation, as judged from the corresponding SF-Abs experiment (Figure 2B, blue trace). The spectrum of the 0.22 s FQ sample (Figure 4B, black bars), when compared to that of the control sample prior to reaction with PetF (blue trace), shows an evident decrease in the area of the resolved quadrupole doublets arising from the $Fe_2^{III/III}$–PHA intermediate. Quantification of the fraction of $Fe_2^{III/III}$–PHA intermediate consumed during the reaction with limiting PetF would distinguish between a one-electron reduction of each reacted ADO intermediate (i.e., decay of 50% of total Fe in the form of the intermediate) or a two-electron reduction (i.e., decay of 25% of total Fe in the form of the intermediate). To quantify this fraction, spectrum A was subtracted from spectrum B (Figure 4C, black bars). The experimental reference spectrum of the $Fe_2^{III/III}$–PHA intermediate was then added back to this direct difference spectrum in intensities ranging from 20 to 50% (Figure S8). The spectrum generated by addition of 25% (Figure 4D) is essentially identical to that of Figure 3E. Moreover, the derived spectra with varying intensities added back are consistent with the analysis of Figure 3E only when the intensity is ≤25% (Figure S8).

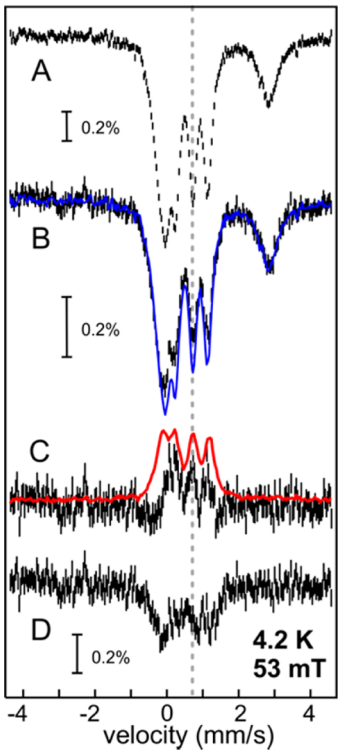

Figure 4. 4.2-K/53-mT FQ-Mössbauer spectra monitoring reduction of the $Fe_2^{III/III}$–PHA intermediate with 0.5 equiv of reduced PetF with respect to ADO. (A) Spectrum of a sample that was freeze-quenched 30 s after a solution of 2 mM $^{57}Fe_2^{II/II}$–ADO, 16.6 mM decanal, and 10 μM Cld was mixed with 10 mM $NaClO_2$. The $Fe_2^{III/III}$–PHA intermediate represents 65% of the total Fe, and the remaining 35% is unreacted $Fe_2^{II/II}$–ADO. (B) Overlay of the spectrum in A (blue line) with the spectrum of a sample freeze-quenched after the $Fe_2^{III/III}$–PHA intermediate, accumulated as in A, was reacted with 0.5 equiv (with respect to ADO) chemically reduced PetF for 0.22 s (black bars). (C) Overlay of the B–A difference spectrum (black bars) with the negative of the experimental reference spectrum of the $Fe_2^{III/III}$–PHA intermediate[10] (red line) plotted at an intensity corresponding to 25% of the total area of the experimental spectrum in B. (D) Spectrum after addition of 25% of the experimental reference spectrum of the $Fe_2^{III/III}$–PHA intermediate to the difference spectrum C. The dashed line denotes the position of the high-energy line of the doublet with ΔE_Q = 0.49 mm/s from the spectrum of the $Fe_2^{III/III}$–PHA intermediate.

Therefore, the fraction of the $Fe_2^{III/III}$–PHA intermediate that reductively decayed upon reaction with limiting PetF is consistent with the rapid, sequential two-electron reduction of each reacted ADO molecule.

Accumulation of Radicals upon Reduction of the $Fe_2^{III/III}$–PHA Intermediate. Considering that PetF is an obligatory one-electron donor, we anticipated that one or more intermediate might accumulate between the two sequential electron transfers in the proposed ADO mechanism. We further expected that, because the reduction of the $Fe_2^{III/III}$–PHA intermediate by PetF is significantly faster than its reduction by ^{MeO}PMS, an ADO intermediate with a half-integer electronic spin state might accumulate to a greater extent with the protein reductant. Therefore, sequential-mixing FQ experiments were carried out with both reducing systems to test for accumulation of EPR-active intermediates during turnover. The reaction times for the FQ-EPR experiments were selected on the basis of the results of the SF-Abs experiments in which the $Fe_2^{III/III}$–

DOI: 10.1021/jacs.5b06345
J. Am. Chem. Soc. 2015, 137, 11695–11709

PHA intermediate was reduced either with equimolar reduced ^{MeO}PMS or with 2 equiv of chemically reduced PetF (Figure 2C).[10]

Upon freeze-quenching of the reaction with either reductant after 0.010 s, a nearly axial EPR signal with principal *g*-values 2.037, 2.009, and 2.003 (Figure 5, black trace; Figure S9) was

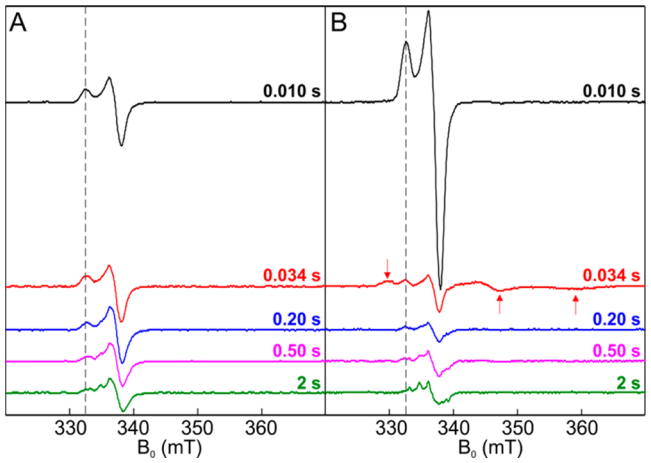

Figure 5. CW EPR spectra of FQ samples obtained after reduction of the $Fe_2^{III/III}$–PHA intermediate by (A) 1 equiv of reduced ^{MeO}PMS or (B) 2 equiv of chemically reduced PetF with respect to ADO. The $Fe_2^{III/III}$–PHA intermediate was accumulated in an initial reaction of the $Fe_2^{II/II}$–ADO·decanal complex with the Cld/$NaClO_2$ system (Figure S2C) and was then mixed with the dithionite-reduced ^{MeO}PMS or PetF. Reaction times were selected on the basis of SF-Abs data shown in Figure 2C. The dashed lines are positioned at the low field feature (g = 2.037) of the transient radical signal. The arrows indicate the features of the $[2Fe\text{-}2S]^{1+}$ PetF cluster signal. Experimental conditions: temperature = 20 K, microwave power = 0.2 mW, microwave frequency = 9.481 GHz, modulation amplitude = 0.4 mT.

detected at temperatures ≤70 K (we did not attempt to collect EPR spectra at higher temperatures because the EPR samples were freeze-quenched and could not be safely annealed to higher temperatures). This radical species did not form if the reducing system was omitted in the second mixing event or if the aldehyde substrate was omitted in the first (Figure S10). With ^{MeO}PMS as the reductant, the S = 1/2 signal accumulated to only <0.05 ADO equivalents at this reaction time. It largely decayed by a reaction time of 0.50 s, as indicated by the greatly diminished intensity of its low-field component at g = 2.037 (Figure 5A, dashed line). Its formation and decay thus occur on the same time scale as ^{MeO}PMS oxidation (Figure 2C, black trace). With 2 equiv of PetF as the reductant, the same EPR signal developed, but to a greater extent. For example, at 0.010 s, ∼0.2 ADO equivalents of the radical species accumulated (Figure 5B, black trace). The yield of the radical was strongly dependent on the stoichiometry of reducing equivalents (Figure 6); its accumulation increased as the PetF:ADO ratio increased to 2, but no further enhancement was seen at greater ratios. The increased accumulation of this transient radical in the reaction with PetF in comparison to the ^{MeO}PMS reaction likely reflects its faster formation with the more potent reductant (Figure 2C, blue trace), which is almost completely oxidized after 0.034 s (as revealed by disappearance of the EPR signal of the PetF $[2Fe\text{-}2S]^{1+}$ form; Figures 5B and S1).

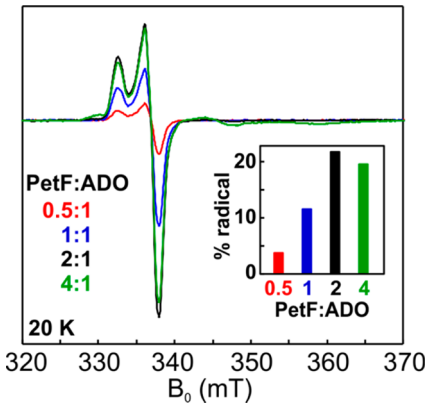

Figure 6. Radical yield as a function of equivalents of PetF with respect to ADO. CW EPR spectra of samples quenched 0.010 s after mixing of the $Fe_2^{III/III}$–PHA intermediate ($[ADO]_{final}$ = 0.23 mM) with varying concentrations of chemically reduced PetF (0.13, 0.23, 0.45, 0.90 mM final concentration). Experimental conditions: temperature = 20 K, microwave power = 0.2 mW, microwave frequency = 9.480 GHz, modulation amplitude = 0.4 mT. (Inset) Yield of the radical species as a function of equivalents of PetF:ADO.

The spectra of samples quenched at reaction times ≥0.034 s exhibited additional S = 1/2 signals that increased in intensity over time (Figure 5). In the ^{MeO}PMS reaction, these signals can be assigned to (a) the phenazine semiquinone radical with an isotropic signal at $g \sim 2$ (Figure S16B), and (b) a second radical species with complex fine structure (Figure 5A, green traces; Figures S11B, S15B), identified on the basis of evidence presented below as a protein-based sulfinyl radical. The same sulfinyl radical signal was present in the spectra of samples from the PetF reaction (Figure 5B, green trace). Its intensity did not depend on the stoichiometry of reducing equivalents, unlike the transient radical EPR signal observed at early time points. The sulfinyl radical accumulated to a much lesser extent, but it was long-lived, persisting for more than 3 min with either reducing system.

Association of the Transient EPR Signal with a Substrate-Derived Alkyperoxyl Radical. The kinetic behavior of the transient radical signal observed in the EPR spectra ($g_{av} \sim 2.02$) and the dependence of its intensity on the reducing system suggest that the associated species might either be, or be derived from, an intermediate in the ADO reaction. The unusual *g*-anisotropy and lack of resolved hyperfine structure in the signal obtained at X-band frequencies weigh against the possibility that the detected species is the purported C2-alkyl radical (the R• resulting from *β*-scission of the *gem*-diolyl radical intermediate; state **E** in Scheme 1).[35−37] To probe the chemical nature of this radical species, identical FQ-EPR experiments were carried out with an aldehyde substrate specifically deuterium-labeled at the C2-position (2,2-$[^2H]_2$-decanal). The EPR signal of a sample generated with this substrate isotopologue exhibited a pronounced line narrowing (Figure 7, red). This effect of replacement of protium results from the smaller hyperfine coupling of deuterium (A_{1H}/A_{2H} = $g_{n(1H)}/g_{n(2H)}$ = 6.514) and proves that the radical is coupled to the C2-hydrons. The radical must therefore be derived from the substrate. Additional experiments carried out with ^{57}Fe-labeled ADO and 1-$[^{13}C]$-labeled octanal did not yield any detectable differences in the spectra (Figure S11A). These observations imply that the radical species is not magnetically coupled to the

DOI: 10.1021/jacs.5b06345
J. Am. Chem. Soc. 2015, 137, 11695−11709

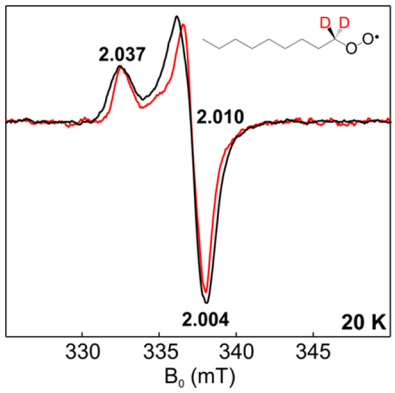

Figure 7. CW EPR spectra of the substrate-derived peroxyl radical species (chemical structure shown in inset). The $Fe_2^{III/III}$–PHA intermediate was formed in the presence of either the 2,2-$[^1H]_2$-decanal (black) or 2,2-$[^2H]_2$-decanal (red) substrate and was reacted with equimolar reduced ^{MeO}PMS for 0.010 s. The spectrum of the 2,2-$[^1H]_2$-decanal sample was multiplied by a factor of 1.7 for better comparison to the spectrum of the 2,2-$[^2H]_2$-decanal sample, because the latter sample had an initial [ADO] 1.7 times greater (1.49 vs 0.90 mM). Experimental conditions: temperature = 20 K, microwave power = 0.2 mW, microwave frequency = 9.480 GHz, modulation amplitude = 0.4 mT.

diiron center and that the C1–C2 bond is cleaved prior to its formation.

The *g*-anisotropy of the substrate-derived radical is reminiscent of signals of peroxyl radicals in proteins and organic systems.[38−44] We posited that the radical could result from the reaction of the proposed R• with dioxygen, yielding a peroxyl radical (ROO•), which would have an electronic structure consistent with the observed EPR signal. FQ-EPR experiments were thus performed with a 3-thiadecanal analogue to test for perturbations to the EPR signal of the radical species. The EPR spectrum of the radical was essentially the same, with only marginal changes in its principal *g*-values (2.034, 2.009, and 2.005) (Figure S12). This insensitivity to the sulfur substitution is expected for a peroxyl radical, because the spin density resides primarily on the oxygen atoms. The EPR signal of a sample generated with the 2,2-$[^2H]_2$-3-thiadecanal analogue exhibited a smaller but detectable line narrowing, also consistent with coupling of the electron spin to the C2-hydrons (Figure S12).

To measure the hyperfine couplings of the C2-hydrons more precisely, HYSCORE experiments were performed on FQ samples prepared with the 2,2-$[^2H]_2$-decanal and the 2,2-$[^2H]_2$-3-thiadecanal substrates and freeze-quenched after a 0.020 s reaction of the $Fe_2^{III/III}$–PHA intermediate with reduced ^{MeO}PMS. The HYSCORE spectra (Figure S13) recorded at the principal positions of the **g**-tensor ($g_{\|}$ = 2.037 and $g_{\perp}$ ~ 2.01) showed correlations between nuclear frequencies from different electronic manifolds corresponding to ^2H nuclei. The cross peaks centered at the ^2H Larmor frequency showed that the ^2H hyperfine couplings for the putative 1,1-$[^2H]_2$-2-thia-$C_8H_{16}OO$• analogue radical are smaller than those for the 1,1-$[^2H]_2$-$C_9H_{16}OO$• radical (Figure S13). Because the modest anisotropy of these signals restricts orientation selection in the HYSCORE experiments, DFT calculations on geometry-optimized models of the substrate-derived radicals (refer to Supporting Information) were used to guide spectral simulations. The spectra could be reproduced well for both radicals, yielding $A_{iso}(^2H)$ ~ 2.6 MHz for the 1,1-$[^2H]_2$-$C_9H_{16}OO$• considering two equivalent deuterium nuclei. For the thia analogue, the $A_{iso}(^2H)$ was decreased by almost half, and the two deuterons were slightly inequivalent (Table S1), as anticipated for the more electron-withdrawing sulfur and the larger extent of delocalization. The single-point calculations on geometry-optimized models of these radical moieties reproduced both the **g**-tensor and the anisotropy of the **A**-tensor reasonably well (Table S1) and support the proposed structure of the transient radical.

Evidence for Trapping of the C2-Alkyl Radical Intermediate by O_2. The substrate-derived peroxyl radical presumably arises from a side-reaction of the R• with dioxygen, and its yield should therefore depend on the concentration of O_2. In all previously described FQ-EPR experiments, a high [O_2] (5 mM after the first mix) was generated by the Cld/$NaClO_2$ enzymatic system.[33,34] In a FQ-EPR experiment with Cld/$NaClO_2$, a ratio of 1:1 PetF:ADO, and octanal as substrate, 0.04 ADO equivalents of the peroxyl radical accumulated after reaction of the $Fe_2^{III/III}$–PHA intermediate with the reduced PetF for 0.010 s (Figure 8A, black spectrum). In contrast, with an O_2-saturated buffer solution (0.90 mM O_2 after the first mix)

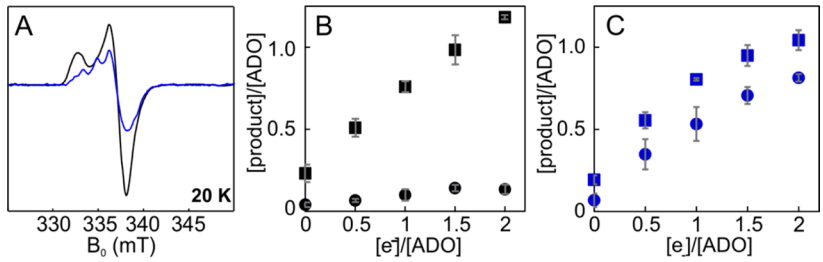

Figure 8. Peroxyl radical and alkane yields in stoichiometric reactions under conditions of excess or limiting O_2. (A) CW EPR spectra of FQ samples generated by reaction of the $Fe_2^{III/III}$–PHA intermediate with 1 equiv of reduced PetF for 0.010 s. The $Fe_2^{III/III}$–PHA intermediate was generated by mixing either the $Fe_2^{II/II}$–ADO·octanal complex (1.49 mM) containing 10 μM Cld with an equal volume of $NaClO_2$ (black line, 10 mM O_2) or the $Fe_2^{II/II}$–ADO·octanal complex (1.49 mM) with O_2-saturated buffer (blue line, 1.8 mM O_2) and incubating for 50 s (Figure S2D). For clarity, the signal of unreacted $[2Fe\text{-}2S]^{1+}$ PetF (15%) was subtracted from these spectra. Experimental conditions: temperature = 20 K, microwave power = 0.2 mW, microwave frequency = 9.480 GHz, modulation amplitude = 0.4 mT. (B, C) Formate (squares) and alkane (circles) product formation in stoichiometric ADO reactions. The $Fe_2^{III/III}$–PHA intermediate was generated by mixing the $Fe_2^{II/II}$–ADO·decanal complex (0.25 mM ADO), in the presence of oxidized FNR and PetF (0.25 mM each), with (B) O_2-saturated buffer (1.8 mM O_2 at 5 °C) and incubating for 10 s or (C) air-saturated buffer (~0.28 mM O_2 at 25 °C) and incubating for 20 s (Figure S2B). The intermediate was then mixed with varying concentrations of NADPH (a two-electron donor) and quenched after ~1 s.

DOI: 10.1021/jacs.5b06345
J. Am. Chem. Soc. 2015, 137, 11695−11709

sufficient to generate an equal quantity of the $Fe_2^{III/III}$–PHA intermediate (Figure S2D), significantly less peroxyl radical accumulated (<0.005 ADO equivalents; see Figure S16B for the spectral deconvolution analysis). The peroxyl radical was barely detectable in the EPR spectrum (Figure 8A, blue spectrum), which was dominated by the signal of the aforementioned sulfinyl radical. The dependence of the quantity of peroxyl radical on the O_2 concentration supports the hypothesis that it is produced from a reaction of the R• with excess molecular oxygen. This reaction appears to be dependent upon the substrate chain-length, with shorter aldehyde substrates (i.e., C_{6-10}) supporting greater accumulation and longer aldehydes (i.e., *n*-octadecanal) supporting minimal accumulation (Figure S14).

If the formation of the peroxyl radical results from the trapping of the R• intermediate by O_2 in competition with its quenching by H•, then the alkane yield (relative to formate) should be diminished by this pathway. Indeed, in single turnover assays under O_2-saturating conditions, the slope of alkane produced versus electrons provided, 0.11 alkane per 2 electrons (Figure 8B), was markedly less than that obtained under O_2-limiting conditions, 0.76 alkane per 2 electrons (Figure 8C). The change in O_2 concentration did not affect the formate yield, which remained essentially identical, irrespective of the quantity of O_2. The significant uncoupling between formate and alkane products observed when O_2 is in excess is consistent with diversion of some of the R• to peroxyl radical, which is expected to decay to an oxidized product. When O_2 was limiting, less R• was unproductively trapped, and, consequently, the alkane:formate ratio approached the theoretical 1:1 stoichiometry.

Detection of a Second Radical Species with Short-Chain Aldehydes. A second EPR-active species was detected in the FQ experiments with short-chain (C_{6-10}) substrates (Figure 5, S15A). This species persisted long after complete oxidation of the ^{MeO}PMS or PetF (>3 min), in contrast to the rapidly decaying peroxyl radical, and could also be detected at temperatures $\lesssim$ 70 K (at least). In FQ-EPR experiments with a ratio of 2:1 PetF:ADO and octanal as substrate, this radical signal detectably accumulated by a reaction time of 0.010 s and was still observed at 2 s, with maximal accumulation to 0.04 ADO equivalents (Figure S15A). The signal of the peroxyl radical developed to only a minor extent in this reaction (Figure S15A, S16). The octanal substrate afforded faster accumulation of this radical than decanal. Further extending this dependence on chain length, the longer, native substrate, *n*-octadecanal, afforded no detectable accumulation of this radical species (Figure S14).

To address the chemical nature of this radical, the aforementioned substrate and cofactor isotopologues were again deployed. However, the EPR signal was not perturbed by using isotopically labeled aldehyde substrates (i.e., 1-[^{13}C]-octanal or 2,2-[^{2}H]$_2$-decanal) nor ^{57}Fe-labeled ADO (Figure S11B), indicating that the radical is neither substrate-derived nor magnetically coupled to the ADO diiron cofactor. Its accumulation was dependent upon the presence of a reducing system but not on the nature of the reducing system (chemical or protein). Collectively, these characteristics suggested that this second, long-lived radical most likely resides on an amino acid residue of ADO.

Assignment of the Second Species as a Sulfinyl Radical on Cys71. The anisotropy and fine structure of the second radical signal do not match known signals of amino acid radicals.[45−47] Its spectral features imply that the spin density resides on an atom with appreciable spin−orbit coupling, such as a sulfur or an oxygen atom.[48,49] Four residues, Tyr18, Tyr22, Cys71, and Tyr123, were identified as candidates to harbor this second radical and were replaced by redox-inert residues (Tyr → Phe or Cys → Ala) to test for elimination of the associated EPR signal. These residues were selected on the basis of their proximity to the bound substrate (Figure 9A) and their strict conservation in cyanobacterial ADO primary structures. In sequential-mixing FQ-EPR experiments, the wild-type (WT) or variant $Fe_2^{II/II}$–ADO·octanal complex was first reacted with the Cld/$NaClO_2$ system to generate the $Fe_2^{III/III}$–PHA intermediate, and the intermediate was then reacted in a second mixing step with equimolar reduced ^{MeO}PMS for 4 s. The EPR spectrum of the WT ADO sample exhibited the complex anisotropic $S = 1/2$ radical signal with an integrated intensity corresponding to 0.08 ADO equivalents. This radical species was formed in all of the ADO variants except C71A (Figure 9B), suggesting that the radical must reside on Cys71. The Tyr → Phe substitutions each resulted in a 2-fold decrease in the radical yield, as well as changes in the signal line shape (Figure 9B). These effects most likely arise from minor perturbations to the environment of the nearby Cys71 residue and radical derived therefrom. In contrast, substitutions of residues located far from Cys71 (e.g., C107A, C117A) resulted in less pronounced changes in the radical signal (Figure S15B). All four variant proteins with substitutions that affected accumulation of the Cys71-based radical are less active than wild-type ADO (i.e., Y18F, 57%; Y22F, 77%; Y123F, 36%; C71A, 73%) under multiple turnover conditions (Table S2); however, no substitution resulted in complete loss of activity.

To resolve the **g**-tensor and fine structure of the Cys71-based radical, the two-pulse echo-detected field-swept Q-band EPR absorption spectrum was recorded. Its first derivative is shown in Figure 9C. The spectrum was simulated with a slightly anisotropic **g**-tensor (g_1, g_2, g_3 = [2.02, 2.01, 2.00]); the "triplet-like" hyperfine structure was reproduced considering two slightly inequivalent ^{1}H hyperfine couplings (A_{iso1} = 39.7 MHz, A_{iso2} = 44.3 MHz). The signal is much less anisotropic than those of thiyl radicals (S•).[48,50] Comparison with studies on sulfur-based radicals reveals that the observed *g*-anisotropy is typical of (alkyl)-sulfinyl radicals (RSO•).[51] There is ample precedent for the production of long-lived sulfinyl radicals from reactions of peroxyl radicals with protein cysteine residues.[38,40,52] The Cys71 sulfinyl radical could thus form from the observed substrate-derived peroxyl radical. Consistent with this deduction, the C71A substitution markedly stabilized the peroxyl radical; after reduction of the $Fe_2^{III/III}$–PHA intermediate for 0.010 s, much more of the peroxyl radical was present in the C71A variant than in the wild-type protein (Figure S16A), and it was still present after a 4 s reaction in the variant protein (Figure 9B, red trace). Sulfinyl radicals typically exhibit EPR signals reflecting a strong hyperfine interaction with only one of the two β-hydrogens.[38,40,52,53] In contrast, the spectrum of the Cys71-based radical reflects appreciable and very similar hyperfine coupling constants for both β-hydrogens. Considering that the spin density on the two hydrogens is very sensitive to the H–C_β–S–O dihedral angle, constraints on this angle imposed by the protein environment in the putative Cys71-SO• might account for the differences in the EPR signal line shape (Figure S18). Indeed, theoretical calculations showed that, at a 120° torsion angle, the experimentally measured hyperfine coupling constants can be well reproduced (Table S3,

DOI: 10.1021/jacs.5b06345
J. Am. Chem. Soc. 2015, 137, 11695−11709

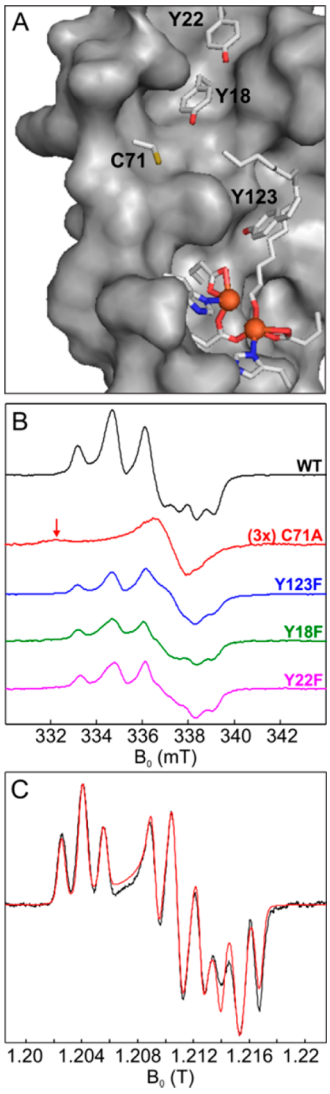

Figure 9. Formation of a Cys71-SO• upon reduction of the $Fe_2^{III/III}$–PHA intermediate. (A) X-ray crystal structure of *Se* ADO (PDB accession code: 4RC5), cut away to depict the location of the residues substituted by mutagenesis (*Np* ADO numbering) relative to the cofactor and bound substrate analogue. (B) CW X-band EPR spectra of freeze-quenched samples from the WT and variant ADO reactions in which the $Fe_2^{II/II}$–ADO·octanal complex ($[ADO]_{final}$ = 0.225 mM WT, C71A and Y123F, 0.150 mM Y18F, and 0.125 mM Y22F) containing Cld was mixed with an equal volume of $NaClO_2$ solution and reacted for 30 s to generate the $Fe_2^{III/III}$–PHA intermediate. Samples were quenched 4 s after a second equal-volume mix of the intermediate with equimolar reduced ^{MeO}PMS. For the Y18F and Y22F variants, the spectra were scaled by factors of 1.8 and 1.5, respectively, for purposes of comparison. The spectrum for the C71A variant was scaled by a factor of 3 for better visualization of the low field component of the ROO• signal (g = 2.037, arrow). Experimental conditions: temperature = 60 K, microwave power = 2 mW, microwave frequency = 9.480 GHz, modulation amplitude = 0.4 mT. (C) First derivative of the two-pulse echo-detected, field-swept Q-band EPR spectrum of the WT ADO 4 s FQ sample. The experimental spectrum (black) was simulated (red) with parameters described in the text. The small discrepancy between the simulation and the experimental spectrum is due to the contribution of the ^{MeO}PMS semiquinone radical signal at $g \sim 2$ and presumably relaxation effects not present in the CW EPR spectrum. Experimental conditions: temperature = 20 K, microwave frequency = 34.08 GHz, shot repetition time (SRT) = 0.5 ms, $\pi/2$ = 12 ns, τ = 328 ns.

Figure S17), corroborating the assignment of this EPR signal as a sulfinyl radical located on Cys71.

DISCUSSION

The Cyanobacterial [2Fe-2S] Fd, PetF, Is an Efficient Reductant for ADO. ADO activity is dependent upon a continuous supply of electrons, both for reduction of the $Fe_2^{III/III}$ form of the cofactor back to the O_2-reactive $Fe_2^{II/II}$ state and during conversion of the $Fe_2^{III/III}$–PHA intermediate state to the product complex. Although artificial chemical reductants (phenazines) have been invaluable tools in elucidating the nature of the ADO reaction and dissecting its mechanism,[9,10,19] they are not viable candidates to serve as the reductant for ADO in a bioprocess producing renewable hydrocarbon fuels. They are kinetically inefficient, do not support robust, stable activity over many turnovers,[9,19] and would present cost and toxicity issues if added to cultures.[54] A biological electron donor would seem to be an essential component of any such bioprocess. The genes encoding ADO and AAR are frequently cotranscribed, but there is no other gene associated with this operon that could encode for a protein to serve as a specific electron donor to ADO.[55] A priori, the in vivo reductant could be either a small biomolecule or a cytosolic redox protein. There is substantial precedent for [2Fe-2S] Fds serving this function for other FDCOOs. Soluble methane monooxygenase (sMMO) employs an iron–sulfur, flavin-containing reductase (sMMOR) that uses NADH to reduce FAD and transfers the two electrons, one at a time, via a plant-type [2Fe-2S] cluster to the nonheme diiron cofactor in the hydroxylase component (sMMOH).[56,57] Other bacterial multicomponent monooxygenases (e.g., toluene/*o*-xylene monooxygenase) have reductase components analogous to sMMOR to service their nonheme diiron hydroxylase components.[58] In the *Ec* class Ia ribonucleotide reductase (RNR), the [2Fe-2S] Fd, YfaE, is required to reduce the μ-oxo-$Fe_2^{III/III}$ cluster in the inactive "met" form of the β subunit to the O_2-reactive $Fe_2^{II/II}$ state to support regeneration of the catalytically essential tyrosyl radical in a process referred to as the "maintenance pathway".[59] In stearoyl-ACP desaturase (Δ^9D), activity depends on an abundant, general plant-type [2Fe-2S] Fd.[60,61] These precedents suggest that the in vivo reductant for ADO might also be a ferredoxin.

Although only modest activity was obtained with a spinach [2Fe-2S] Fd,[4,20] it is likely that differences between the plant and cyanobacterial proteins in regions of contact with ADO might be responsible for the inefficiency of the heterologous plant Fd. We tested seven predicted Fd proteins encoded within the fully sequenced genome of the alkane-producing, model cyanobacterium *Syn.* 6803 for their ability to support alkane production in in vitro reactions containing stearoyl-ACP, *Np* AAR, and *Np* ADO. The Fd encoded by the gene *ssl0020*, annotated as PetF or FdI, was identified as the most efficient reducing partner in these multiple-turnover assays. PetF was reported to support in vivo propane production in an engineered microbial platform, employing *Prochlorococcus marinus* AAR/ADO in *Ec* as a host.[22,62] In addition, its closest orthologue in *Se* (75% sequence identity) was shown to afford faster ADO turnover in vitro than the phenazine system.[20] PetF is the most abundant of the *Syn.* 6803 Fds and is essential for cell viability.[32,63] The cellular abundance of PetF, together with the results demonstrating its suitability as an electron donor to ADO, suggest that it might be the physiological donor and provide the rationale for the use of this one-electron reducing

DOI: 10.1021/jacs.5b06345
J. Am. Chem. Soc. 2015, 137, 11695–11709

system to probe details of the ADO mechanism that have not been accessible with chemical two-electron donors.

High Product Yield via the Complete PetF/FNR/N System. The efficiency of PetF as an electron donor was established, first, by examining the product:electron stoichiometry. In single-turnover experiments employing chemically reduced PetF, the stoichiometry was 0.58 formate:2 electrons, appreciably less than the predicted ratio of 1 formate:2 electrons. In contrast, when the complete PetF/FNR/N system was used, a coupling ratio of 0.96 formate:2 electrons was obtained, essentially achieving the theoretical maximum. In the latter case, the two electrons from NADPH are transferred to the FAD cofactor of FNR and then shuttled sequentially to the PetF [2Fe-2S] cluster, which finally delivers the electrons to the diiron site of ADO one at a time. The enhanced catalytic performance of ADO with the PetF/FNR/N system may result from well-timed electron delivery and avoidance of reductive quenching of reactive intermediates. More controlled delivery of electrons to the ADO diiron site might also help prevent reduction of O_2 to H_2O_2, reported to be an inhibitor of ADO.[20,64]

Kinetic Superiority of PetF as ADO Reductant Relative to Other Systems. *Reduction of the $Fe_2^{III/III}$ Cofactor Form.* PetF can reduce the diferric forms of ADO moderately rapidly, irrespective of whether these forms were generated from productive or unproductive oxidation.[10] In SF-Abs experiments, reduction of the diferric ADO (aerobically isolated or from productive oxidative conversion) occurred with an observed rate constant of 0.8 s^{-1} at 5 °C. This rate constant is similar to those reported for reduction of the $Fe_2^{III/III}$ forms of other FDCOOs by their [2Fe-2S] Fd partners (RNR-β_2 k_{obs1} ∼ 4−5 s^{-1} and k_{obs2} ∼ 1−2 s^{-1} at 37 °C; Δ^9D k_{obs} = 3.4 s^{-1} at 25 °C; sMMOH with the sMMOR Fd domain k_{obs1} = 1 s^{-1} and k_{obs2} = 0.2 s^{-1} at 4 °C).[57,59,60] Considering that the fastest reported multiple-turnover rate for ADO with the PetF/FNR/N reducing system is 0.007 s^{-1} (at 37 °C),[20] reduction of the diferric state(s) by PetF cannot be rate-limiting. The observed rate constant for reduction of diferric ADO by the reduced phenazine is almost 100 times less.[10] PetF is thus the most efficient electron donor to $Fe_2^{III/III}$−ADO reported to date.

Reduction of the $Fe_2^{III/III}$−PHA Intermediate. To support efficient catalysis by ADO, a redox partner protein must not only reduce the $Fe_2^{III/III}$ product form of the ADO cofactor to the reactant $Fe_2^{II/II}$ state but also supply two electrons, one at a time, in precisely timed fashion, to the cofactor site during conversion of the $Fe_2^{III/III}$−PHA intermediate to the product complex. Indeed, SF-Abs experiments demonstrated that reduction of the $Fe_2^{III/III}$−PHA intermediate by PetF is remarkably rapid (k_{obs} > 400 s^{-1} at 5 °C) and is more than 40 times faster than reduction by ^{MeO}PMS (k_{obs} = 9 s^{-1} at 5 °C)[10] under these experimental conditions. In agreement with the more rapid electron donation by PetF, the Mössbauer spectrum of a sample after a 0.010 s reaction of the $Fe_2^{III/III}$−PHA intermediate with PetF is similar to that of a sample after a 0.56 s reaction of the intermediate with ^{MeO}PMS;[10] both spectra reveal disappearance of the $Fe_2^{III/III}$−PHA intermediate to a similar extent. In the PetF reaction, 55% of the total ^{57}Fe in the sample has undergone conversion from the $Fe_2^{III/III}$−PHA intermediate to new $Fe_2^{III/III}$ species in 0.010 s, and, by 0.22 s, the intermediate has completely decayed. At least two distinct $Fe_2^{III/III}$ species formed in the reduction reaction: (a) one species that was not previously observed in the analogous experiment with ^{MeO}PMS as reductant, but is the major component at the shortest reaction time point upon reduction by PetF, and (b) a second one that accumulates at later reaction times and has parameters similar to those of the putative formate-bound complex (state **G** in Scheme 1) previously detected in the reaction with ^{MeO}PMS.[10] The first species presumably represents a state that accumulates only in the PetF reaction as a result of its greater efficiency and perhaps its nature as an obligatory single-electron donor. Although structural assignment of this $Fe_2^{III/III}$-containing species is beyond the scope of the present work, our results nevertheless demonstrate that reductive decay of the $Fe_2^{III/III}$−PHA intermediate is accompanied by formation of only diferric species, strongly supporting the mechanism in Scheme 1.

In the SF-Abs experiment performed with a ratio of 0.5:1 PetF:ADO, the kinetic trace at 423 nm (absorption increase reflecting PetF $[2Fe\text{-}2S]^{1+}$ oxidation) exhibited a decay phase after ∼0.5 s. Because PetF cannot be rereduced under these experimental conditions, the observed decay phase must be associated with another chromophore absorbing at this wavelength. Indeed, the observed rate constant is essentially identical to that of the unproductive decay of the $Fe_2^{III/III}$−PHA intermediate, which has an absorption maximum at 450 nm (ε_{450} = 1 200 $M^{-1}\cdot cm^{-1}$).[10] This observation suggests that when PetF is substoichiometric with respect to ADO, two electrons are rapidly transferred to one ADO molecule, such that a portion of the $Fe_2^{III/III}$−PHA is not reduced at all. The notion of rapid, consecutive electron transfers is corroborated by the Mössbauer spectrum of a sample generated using the same ratio of PetF:ADO (0.5:1), in which the $Fe_2^{III/III}$−PHA intermediate was reacted with reduced PetF for 0.22 s. This spectrum showed that no more than 25% of the ADO reacted under these conditions, establishing that two electrons are shuttled (sequentially) to a single diiron site. In stoichiometric reactions of the $Fe_2^{III/III}$−PHA intermediate with PetF/FNR/N, the stoichiometry of formate:electrons observed was ∼0.5:1, as opposed to the 1:1 ratio expected if each ADO molecule were to be reduced by just one electron, considering that formate is generated after only a single electron transfer. The observed stoichiometry thus corroborates that half of the $Fe_2^{III/III}$−PHA intermediate reacts to consume two reducing equivalents. The rapid, tightly coupled delivery of two electrons (sequentially) to the $Fe_2^{III/III}$−PHA intermediate demonstrates that PetF can function as an effective redox partner for ADO, optimally timing electron transfer events for efficient substrate conversion.

The results of the FQ Mössbauer and EPR experiments probing reduction of the $Fe_2^{III/III}$−PHA intermediate by the obligatory single-electron donor, PetF, also demonstrate that only diferric intermediate states accumulated during substrate conversion, in agreement with our previous studies with the phenazine system.[10] We obtained no spectroscopic evidence for accumulation of a diferrous or a mixed-valent species upon reduction of the $Fe_2^{III/III}$−PHA intermediate by PetF, providing argument against an alternative mechanism involving such intermediates that was proposed by another group.[15] Likewise, no evidence was obtained for formation of high-valent intermediates (i.e., analogous to "X" in class Ia RNR or "Q" in sMMOH) during the reaction, although such species could still possibly form on the ADO reaction pathway but fail to accumulate to detectable levels because of unfavorable kinetics. However, generation of an "X"-like species can be excluded by our FQ-EPR results, thus weighing against a proposed mechanism involving heterolytic O−O and C1−C2 bond

DOI: 10.1021/jacs.5b06345
J. Am. Chem. Soc. 2015, 137, 11695−11709

cleavage.[18] The accumulation of only diferric species provides strong support for the free-radical mechanism previously proposed by us and shown in Scheme 1.[5,10]

Evidence for a Free-Radical Mechanism and Ineffective Containment of Intermediates. *A Peroxyl Radical Derived from the C2-Alkyl Radical.* According to Scheme 1, reductive cleavage of the peroxyhemiacetal moiety in state **C** would result in generation of R•, a C2-alkyl radical intermediate, in the free-radical mechanism. In FQ-EPR experiments following the reduction of the $Fe_2^{III/III}$–PHA intermediate by either ^{MeO}PMS or PetF, formation of a transient radical was observed but with spectroscopic features different from those expected for the R•.[35−37] By isotopic labeling of the substrate and cofactor, this species was identified as a substrate-derived peroxyl radical (ROO•) that forms after C1−C2 scission and that is not magnetically coupled to the diiron center. The extent and kinetics of accumulation of the ROO• depended sensitively upon the presence, stoichiometry, and nature of the reductant, strongly suggesting that the ROO• is related to an intermediate in the reaction. The fact that its level of accumulation is positively correlated with the concentration of O_2 present during the reaction and negatively correlated with alkane yield suggests that it is a byproduct of the combination of the proposed R• with molecular oxygen.

Peroxyl radicals are well documented in enzymes operating by free-radical mechanisms. They are typically generated by reaction of carbon-centered radicals with molecular oxygen.[65−69] Known ROO• species in these systems have either catalytic or inhibitory roles.[38,39] In purple lipoxygenases, an ROO• is the on-pathway intermediate in the dioxygenative conversion of linoleic acid to hydroperoxy-octadecadienoic acid.[39,41,42] In the Y122F variant of *Ec* RNR β, but not in the wild-type enzyme, formation of an amino acid-derived peroxyl radical was observed, presumably due to the imperfect containment of free-radical intermediates.[70] Perhaps the best characterized ROO• adduct is the one observed in pyruvate formate-lyase (PFL), in which the catalytic glycyl radical reacts with O_2 to form a peroxyl radical that initiates cleavage of the peptide backbone, ultimately inactivating the enzyme.[38,52] The formation of a substrate-derived peroxyl radical during the productive reaction of ADO via quenching of an on-pathway intermediate unequivocally establishes that the enzyme operates by a free-radical mechanism.

A Cys71-Centered Sulfinyl Radical in the Reaction of ADO with Short-Chain Substrates. The substrate-derived ROO• in ADO decayed rather quickly. After a reaction time of 0.50 s, it was hardly detectable and a second radical signal had developed. FQ-EPR experiments with ADO variants and aldehyde isotopologues identified that this second radical is located on residue Cys71 of ADO. The *g*-anisotropy of its EPR signal and its fine structure, however, are not consistent with those reported for cysteine thiyl radicals.[48,50] Comparison with other sulfur-based radicals identified its chemical structure as a sulfinyl radical (RSO•).[38,40,51,52] Despite the similar *g*-anisotropy, its fine structure differs from that typical of other RSO• species, which exhibit one large and one small hyperfine coupling for the two β-hydrogens.[38,40,52,53] This difference is rationalized by an unusual H−C_β−S−O dihedral angle, which is known to impact spin density on the two β-hydrogens.[71] Theoretical calculations show that the experimentally observed hyperfine coupling constants can be reproduced by a particular torsion angle, corroborating the assignment of this signal as a Cys71-SO• species. The rotation about the C−S bond needed to achieve this unusual angle may be enforced by the hydrophobic substrate-binding pocket and the interaction of the Cys71-SO• with a nearby phenylalanine residue (see SI).

Sulfinyl radicals are known to form in reactions of peroxyl radicals with nearby cysteine residues in both PFL and class Ia RNR.[38,40,52] In ADO, the kinetics of formation of the Cys71-SO• suggest that it is generated from a similar reaction of the substrate-derived ROO• with Cys71. Indeed, in the C71A variant, the peroxyl radical accumulated to a greater extent than in the wild-type protein at 0.010 s and was still detectable after 4 s. The extent and the kinetics of Cys71-SO• accumulation were strongly dependent on the chain-length of the aldehyde substrate. Considering that Cys71 is far from the active site and gates the hydrophobic substrate channel,[1,72,73] the peroxyl radical must migrate within the active site for this reaction to occur. Short-chain substrates are expected to have greater mobility, explaining the observed more rapid and greater accumulation of the Cys71-SO•. However, the fact that less Cys71-SO• product than ROO• precursor accumulated, together with the decay kinetics of ROO•, imply that a fraction of the ROO• decayed by one or more than one alternative pathway. At present, the nature of the other decay route(s) and whether the formation of Cys71-SO• partially or completely inactivates ADO remain unclear.[74]

Unproductive Quenching of the C2-Alkyl Radical by Excess O_2. Detection of a substrate-derived ROO• reveals a limited competency of ADO to contain its free-radical intermediate, R•. The extent of ROO• formation was strictly dependent on the concentration of O_2 present during reduction of the $Fe_2^{III/III}$–PHA intermediate, as demonstrated in FQ-EPR experiments with different residual concentrations of O_2 after its consumption as a cosubstrate (generating comparable amounts of the intermediate). The higher yield of ROO• was strongly correlated with the diminished alkane yields observed in such stoichiometric reactions. When O_2 was limited to prevent formation of the ROO•, the alkane yield approached the expected stoichiometry of unity with the formate coproduct. The latter is formed after C1−C2 scission, and its yield is independent of the O_2 concentration, as expected. These results demonstrate that, in the presence of excess O_2, an appreciable fraction of the R• intermediate is lost as ROO•, ultimately precluding its productive conversion to alkane.

Therefore, although molecular oxygen is absolutely essential for the ADO reaction, it can also limit the yield of the desired alkane product. This observation has, in fact, been reported previously in both in vitro and in vivo studies, but the molecular origins were not identified. In an in vitro study employing the phenazine reducing system, alkane production was greatly enhanced under microaerobic conditions; yields were otherwise very low in the presence of excess O_2 (~30-fold relative to [ADO]).[17] More recently, in a bioengineered *Ec* system overexpressing ADO, the PetF/FNR system, and catalase, production of short-chain alkanes (e.g., propane and heptane) was inhibited by excess O_2. In contrast, when the O_2 concentration was significantly decreased, alkane production was enhanced.[22] The poor alkane yield was thus found to be independent of the nature of the reducing system (chemical or protein) and of whether the reaction takes place in vitro or in vivo. These observations are in agreement with our experimental results, which clearly demonstrate that the molecular basis for the diminished alkane production is the previously unrecognized unproductive trapping of the R• intermediate by excess O_2.

DOI: 10.1021/jacs.5b06345
J. Am. Chem. Soc. 2015, 137, 11695−11709

Accumulation of off-pathway radical species was more pronounced with short-chain aldehydes (e.g., C_{6-10}). This phenomenon is particularly important because short-chain alkanes have been specifically targeted for their uses as liquefied petroleum gas (e.g., propane and butane) and as "drop-in" gasoline and jet-fuel components (e.g., heptane to undecane).[22,62,75] Short-chain aldehydes are also superior substrates for ADO in vitro compared to the natural long-chain substrates, due to their greater solubility.[9,10,19] Thus, bioengineered ADO variants have been designed to favor short-chain substrates by sterically occluding the substrate channel, demonstrating higher activity with aldehydes as short as butanal both in vitro and in vivo.[75] In this work, we show that, in the presence of excess O_2 and/or short-chain aldehydes, the alkane yields are greatly compromised because ADO lacks an efficient mechanism to productively quench its radical intermediate. Our results establish that ADO employs a free-radical mechanism for conversion of fatty aldehydes to alkanes, and that, although O_2 is a cosubstrate, it also exposes the Achilles heel of this enzyme. Limiting flux through the unproductive pathways identified here would be a worthwhile goal in efforts to develop more efficient ADO-based bioprocesses.

■ ASSOCIATED CONTENT

Supporting Information

The Supporting Information is available free of charge on the ACS Publications website at DOI: 10.1021/jacs.5b06345.

Scheme S1 with procedures for syntheses of aldehyde substrates and analogues, complete procedures for protein preparations, and Cartesian coordinates for DFT calculations of radical models, Tables S1−S3 with theoretical and experimental analyses, and Figures S1−S18 containing spectra from SF-Abs, Mössbauer and EPR experiments with additional spectral analysis (PDF)

■ AUTHOR INFORMATION

Corresponding Authors

*mxp65@psu.edu
*jmb21@psu.edu
*cdk10@psu.edu
*sjb14@psu.edu

Present Addresses

[§]Novo Nordisk A/S, Novo Nordisk Park 1, Måløv, Denmark.
[⊥]Joule Unlimited Technologies, Inc., 18 Crosby Dr., Bedford, MA 01730.

Notes

The authors declare no competing financial interest.

■ ACKNOWLEDGMENTS

We thank Ashley Compton (Massachusetts Institute of Technology) for her assistance in the initial experiments with PetF. This work was supported by the National Science Foundation (MCB-1122079 to C.K., J.M.B., S.J.B.) and LS9, Inc.

■ REFERENCES

(1) Schirmer, A.; Rude, M. A.; Li, X.; Popova, E.; del Cardayre, S. B. *Science* **2010**, *329*, 559.
(2) Lin, F. M.; Das, D.; Lin, X. N.; Marsh, E. N. G. *FEBS J.* **2013**, *280*, 4773.
(3) Warui, D. M.; Pandelia, M.-E.; Rajakovich, L. J.; Krebs, C.; Bollinger, J. M., Jr.; Booker, S. J. *Biochemistry* **2015**, *54*, 1006.
(4) Warui, D. M.; Li, N.; Nørgaard, H.; Krebs, C.; Bollinger, J. M., Jr.; Booker, S. J. *J. Am. Chem. Soc.* **2011**, *133*, 3316.
(5) Li, N.; Nørgaard, H.; Warui, D. M.; Booker, S. J.; Krebs, C.; Bollinger, J. M., Jr. *J. Am. Chem. Soc.* **2011**, *133*, 6158.
(6) Akhtar, M. K.; Turner, N. J.; Jones, P. R. *Proc. Natl. Acad. Sci. U. S. A.* **2013**, *110*, 87.
(7) Schirmer, A.; Rude, M. A.; Brubaker, S. (LS9) Int. Patent WO/2009/140696, 2009.
(8) Reppas, N. B.; Ridley, C. P. (Joule Unlimited, Inc.) US Patent US 7794969 B1, 2010.
(9) Li, N.; Chang, W.-c.; Warui, D. M.; Booker, S. J.; Krebs, C.; Bollinger, J. M., Jr. *Biochemistry* **2012**, *51*, 7908.
(10) Pandelia, M.-E.; Li, N.; Nørgaard, H.; Warui, D. M.; Rajakovich, L. J.; Chang, W.-c.; Booker, S. J.; Krebs, C.; Bollinger, J. M., Jr. *J. Am. Chem. Soc.* **2013**, *135*, 15801.
(11) Krebs, C.; Bollinger, J. M., Jr.; Booker, S. J. *Curr. Opin. Chem. Biol.* **2011**, *15*, 291.
(12) Merkx, M.; Kopp, D. A.; Sazinsky, M. H.; Blazyk, J. L.; Müller, J.; Lippard, S. J. *Angew. Chem., Int. Ed.* **2001**, *40*, 2782.
(13) Wallar, B. J.; Lipscomb, J. D. *Chem. Rev.* **1996**, *96*, 2625.
(14) Moënne-Loccoz, P.; Baldwin, J.; Ley, B. A.; Loehr, T. M.; Bollinger, J. M., Jr. *Biochemistry* **1998**, *37*, 14659.
(15) Waugh, M. W.; Marsh, E. N. G. *Biochemistry* **2014**, *53*, 5537.
(16) Paul, B.; Das, D.; Ellington, B.; Marsh, E. N. G. *J. Am. Chem. Soc.* **2013**, *135*, 5234.
(17) Das, D.; Ellington, B.; Paul, B.; Marsh, E. N. G. *ACS Chem. Biol.* **2014**, *9*, 570.
(18) Aukema, K. G.; Makris, T. M.; Stoian, S. A.; Richman, J. E.; Münck, E.; Lipscomb, J. D.; Wackett, L. P. *ACS Catal.* **2013**, *3*, 2228.
(19) Eser, B. E.; Das, D.; Han, J.; Jones, P. R.; Marsh, E. N. G. *Biochemistry* **2011**, *50*, 10743.
(20) Zhang, J.; Lu, X.; Li, J. J. *Biotechnol. Biofuels* **2013**, *6*, 86.
(21) Wang, Q.; Huang, X.; Zhang, J.; Lu, X.; Li, S.; Li, J. J. *Chem. Commun.* **2014**, *50*, 4299.
(22) Kallio, P.; Pasztor, A.; Thiel, K.; Akhtar, M. K.; Jones, P. R. *Nat. Commun.* **2014**, *5*, 4731.
(23) Hagen, W. R. *Dalton Trans.* **2006**, 4415.
(24) Warui, D. M.; Li, N.; Nørgaard, H.; Krebs, C.; Bollinger, J. M., Jr.; Booker, S. J. *J. Am. Chem. Soc.* **2011**, *133*, 3316.
(25) Price, J. C.; Barr, E. W.; Tirupati, B.; Bollinger, J. M., Jr.; Krebs, C. *Biochemistry* **2003**, *42*, 7497.
(26) Jiang, W.; Hoffart, L. M.; Krebs, C.; Bollinger, J. M., Jr. *Biochemistry* **2007**, *46*, 8709.
(27) Ravi, N.; Bollinger, J. M., Jr.; Huynh, B. H.; Edmondson, D. E.; Stubbe, J. *J. Am. Chem. Soc.* **1994**, *116*, 8007.
(28) Stoll, S.; Schweiger, A. *J. Magn. Reson.* **2006**, *178*, 42.
(29) Reijerse, E.; Lendzian, F.; Isaacson, R.; Lubitz, W. *J. Magn. Reson.* **2012**, *214*, 237.
(30) Neese, F. *Wiley Interdiscip. Rev.: Comput. Mol. Sci.* **2012**, *2*, 73.
(31) Gilson, M. K.; Honig, B. *Proteins: Struct., Funct., Genet.* **1988**, *4*, 7.
(32) Poncelet, M.; Cassier-Chauvat, C.; Leschelle, X.; Bottin, H.; Chauvat, F. *Mol. Microbiol.* **1998**, *28*, 813.
(33) Dassama, L. M. K.; Yosca, T. H.; Conner, D. A.; Lee, M. H.; Blanc, B.; Streit, B. R.; Green, M. T.; DuBois, J. L.; Krebs, C.; Bollinger, J. M., Jr. *Biochemistry* **2012**, *51*, 1607.
(34) Krebs, C.; Dassama, L. M. K.; Matthews, M. L.; Jiang, W.; Price, J. C.; Korboukh, V.; Li, N.; Bollinger, J. M., Jr. *Coord. Chem. Rev.* **2013**, *257*, 234.
(35) Kochi, J. K.; Krusic, P. J. *J. Am. Chem. Soc.* **1969**, *91*, 3940.
(36) Ellinger, Y.; Subra, R.; Levy, B.; Millie, P.; Berthier, G. *J. Chem. Phys.* **1975**, *62*, 10.
(37) Fessenden, R. W.; Schuler, R. H. *J. Chem. Phys.* **1963**, *39*, 2147.
(38) Reddy, S. G.; Wong, K. K.; Parast, C. V.; Peisach, J.; Magliozzo, R. S.; Kozarich, J. W. *Biochemistry* **1998**, *37*, 558.
(39) Nelson, M. J.; Cowling, R. A.; Seitz, S. P. *Biochemistry* **1994**, *33*, 4966.
(40) Adrait, A.; Öhrström, M.; Barra, A. L.; Thelander, L.; Gräslund, A. *Biochemistry* **2002**, *41*, 6510.

DOI: 10.1021/jacs.5b06345
J. Am. Chem. Soc. 2015, 137, 11695−11709

(41) Nelson, M. J.; Seitz, S. P.; Cowling, R. A. *Biochemistry* **1990**, *29*, 6897.
(42) Nelson, M. J.; Cowling, R. A. *J. Am. Chem. Soc.* **1990**, *112*, 2820.
(43) Becker, D.; Yanez, J.; Sevilla, M. D.; Alonsoamigo, M. G.; Schlick, S. *J. Phys. Chem.* **1987**, *91*, 492.
(44) Yanez, J.; Sevilla, C. L.; Becker, D.; Sevilla, M. D. *J. Phys. Chem.* **1987**, *91*, 487.
(45) Stubbe, J.; van der Donk, W. A. *Chem. Rev.* **1998**, *98*, 705.
(46) Bleifuss, G.; Kolberg, M.; Potsch, S.; Hofbauer, W.; Bittl, R.; Lubitz, W.; Gräslund, A.; Lassmann, G.; Lendzian, F. *Biochemistry* **2001**, *40*, 15362.
(47) Svistunenko, D. A.; Cooper, C. E. *Biophys. J.* **2004**, *87*, 582.
(48) van Gastel, M.; Lubitz, W.; Lassmann, G.; Neese, F. *J. Am. Chem. Soc.* **2004**, *126*, 2237.
(49) Persson, A. L.; Sahlin, M.; Sjöberg, B.-M. *J. Biol. Chem.* **1998**, *273*, 31016.
(50) Kolberg, M.; Bleifuss, G.; Gräslund, A.; Sjöberg, B.-M.; Lubitz, W.; Lendzian, F.; Lassmann, G. *Arch. Biochem. Biophys.* **2002**, *403*, 141.
(51) Gilbert, B. C. In *Structure and Reaction Mechanisms in Sulphur-Radical Chemistry Revealed by E.S.R. Spectroscopy in Sulphur-Centered Reactive Intermediates in Chemistry and Biology*; Springer: New York, 1990; Vol. *197*.
(52) Zhang, W.; Wong, K. K.; Magliozzo, R. S.; Kozarich, J. W. *Biochemistry* **2001**, *40*, 4123.
(53) Stegmann, H. B. In *Radicals Centered on Heteroatoms with Z > 7 and Selected Anion Radicals I: 10.1.2 Sulfinyl Radicals*; Fischer, H., Ed.; Springer: Berlin, 1988.
(54) Nanayakkara, N. P. D.; Schrader, K. K. *Aquacult. Res.* **2011**, *42*, 1895.
(55) Klahn, S.; Baumgartner, D.; Pfreundt, U.; Voigt, K.; Schon, V.; Steglich, C.; Hess, W. R. *Front. Bioeng. Biotechnol.* **2014**, *2*, 24.
(56) Müller, J.; Lugovskoy, A. A.; Wagner, G.; Lippard, S. J. *Biochemistry* **2002**, *41*, 42.
(57) Blazyk, J. L.; Gassner, G. T.; Lippard, S. J. *J. Am. Chem. Soc.* **2005**, *127*, 17364.
(58) Acheson, J. F.; Bailey, L. J.; Elsen, N. L.; Fox, B. G. *Nat. Commun.* **2014**, *5*, 5009.
(59) Wu, C. H.; Jiang, W.; Krebs, C.; Stubbe, J. *Biochemistry* **2007**, *46*, 11577.
(60) Lyle, K. S.; Haas, J. A.; Fox, B. G. *Biochemistry* **2003**, *42*, 5857.
(61) Sobrado, P.; Lyle, K. S.; Kaul, S. P.; Turco, M. M.; Arabshahi, I.; Marwah, A.; Fox, B. G. *Biochemistry* **2006**, *45*, 4848.
(62) Menon, N.; Pasztor, A.; Menon, B. R.; Kallio, P.; Fisher, K.; Akhtar, M. K.; Leys, D.; Jones, P. R.; Scrutton, N. S. *Biotechnol. Biofuels* **2015**, *8*, 61.
(63) Mazouni, K.; Domain, F.; Chauvat, F.; Cassier-Chauvat, C. *Mol. Microbiol.* **2003**, *49*, 1019.
(64) Andre, C.; Kim, S. W.; Yu, X. H.; Shanklin, J. *Proc. Natl. Acad. Sci. U. S. A.* **2013**, *110*, 3191.
(65) Neta, P.; Huie, R. E.; Ross, A. B. *J. Phys. Chem. Ref. Data* **1990**, *19*, 413.
(66) Alfassi, Z. B. *The Chemistry of Free Radicals: Peroxyl Radicals*; John Wiley & Sons Ltd: West Sussex, England, 1997.
(67) Stark, M. S. *J. Am. Chem. Soc.* **2000**, *122*, 4162.
(68) Bolsman, T. A. B. M.; Brouwer, D. M. *Recl. Trav. Chim. Pays-Bas* **1978**, *97*, 320.
(69) Gilbert, D. L.; Colton, C. A. In *Reactive Oxygen Species in Biological Systems: An Interdisciplinary Approach*; Springer: New York, 2002.
(70) Sahlin, M.; Cho, K. B.; Pötsch, S.; Lytton, S. D.; Huque, Y.; Gunther, M. R.; Sjöberg, B.-M.; Mason, R. P.; Gräslund, A. *JBIC, J. Biol. Inorg. Chem.* **2002**, *7*, 74.
(71) Gordy, W. In *Intrepretation of Nuclean Coupling in Oriented Free Radicals in Theory and Applications of Electron Spin Resonance*; John Wiley and Sons: New York, 1980.
(72) Buer, B. C.; Paul, B.; Das, D.; Stuckey, J. A.; Marsh, E. N. G. *ACS Chem. Biol.* **2014**, *9*, 2584.
(73) Jia, C.; Li, M.; Li, J.; Zhang, J.; Zhang, H.; Cao, P.; Pan, X.; Lu, X.; Chang, W. *Protein Cell* **2015**, *6*, 55.
(74) Hayashi, Y.; Yasugi, F.; Arai, M. *PLoS One* **2015**, *10*, e0122217.
(75) Khara, B.; Menon, N.; Levy, C.; Mansell, D.; Das, D.; Marsh, E. N. G.; Leys, D.; Scrutton, N. S. *ChemBioChem* **2013**, *14*, 1204.

DOI: 10.1021/jacs.5b06345
J. Am. Chem. Soc. 2015, 137, 11695−11709